Perturbing H-NS function reveals roles in restricting virulence heterogeneity and pathogen adaptation

Leah McLelland[1], Dakshya Karki[1], Madison Spratt[1,2], Miracle Burt[1], Jonathan Zhao[1], Keara Lane[1,3]

1 Department of Molecular Biosciences, Northwestern University, Evanston, Illinois, 60208, USA

2 Interdisciplinary Biological Sciences Graduate Program, Northwestern University, Evanston, Illinois, 60208, USA

3 National Institute for Theory and Mathematics in Biology, Northwestern University and The University of Chicago, Chicago, IL, USA

* Corresponding author: Keara Lane (keara.lane@northwestern.edu)

ABSTRACT

Bacterial pathogens must balance rapid expression of virulence genes in host niches with tight repression when not needed to avoid fitness costs and ensure survival. Integration of virulence gene regulatory networks with the conserved global repressor H-NS was critical to achieve this balance. H-NS-mediated repression of virulence genes in non-inducing environments is essential for maintaining virulence genes and has shaped pathogen evolution. However, the role of H-NS-mediated repression in virulence gene activation and pathogen evolution in virulence-inducing conditions is less clear. For instance, although virulence gene expression is often heterogeneous, whether relief of H-NS repression contributes to this heterogeneity remains unknown. Furthermore, whether H-NS repression shapes pathogen evolution in virulence-inducing environments is unclear. Here, we use a *Salmonella* strain with reduced H-NS DNA-binding affinity to investigate the role of H-NS in virulence gene expression in individual bacteria and pathogen adaptation. We find that reduced H-NS repression increases the fraction of virulence gene expressing cells without eliminating bimodality, resulting in enhanced epithelial cell infection *in vitro*. Using experimental evolution, we demonstrate that the *hns* genotype constrains adaptive mutations and that disabling virulence gene expression is a common path to improved fitness in intracellular-like environments. Our results expand the role of H-NS-mediated repression from silencing virulence genes in non-inducing conditions to regulating heterogeneity in inducing conditions and demonstrate that evolutionary conservation of H-NS constrains adaptive strategies in intracellular-like environments.

35 **INTRODUCTION**

36 Bacterial pathogens must rapidly adjust virulence gene expression patterns while colonizing
37 diverse host environments [1–4]. Optimal virulence gene repression is a critical yet challenging
38 part of this process. Excessive repression of virulence genes delays necessary functional
39 responses, such as production of a type III secretion system (T3SS) or toxins, leading to a failure
40 to adapt and survive in a host environment. Conversely, insufficient repression leads to
41 inappropriate virulence gene expression, imposing fitness costs ranging from reduced growth to
42 detection by the immune system [5–7]. To balance these competing demands, bacterial
43 pathogens have evolved regulatory strategies that integrate virulence gene regulatory networks
44 with global repressors, enabling both tight silencing and rapid activation as needed [8–10]. Here,
45 we examine how perturbing one such global repressor, histone-like nucleoid structuring protein
46 (H-NS), affects virulence gene expression heterogeneity and evolutionary adaptation in the
47 intracellular bacterial pathogen *Salmonella enterica* serovar Typhimurium (STm).

48 H-NS is a global repressor of gene expression in Gram-negative bacteria, including STm [10,11].
49 It is an abundant nucleoid-associated protein composed of an N-terminal oligomerization domain
50 and a C-terminal DNA-binding domain (DBD) connected via a flexible linker. The DBD
51 preferentially binds to curved AT-rich DNA sequences, while the oligomerization domain enables
52 higher-order complex formation that compacts and bridges DNA [12–17]. By binding AT-rich
53 promoters, including horizontally-acquired virulence genes, H-NS occludes RNA polymerase and
54 thereby blocks transcription [16,18].

55 H-NS-mediated repression is essential for STm viability. Loss of *hns* causes widespread
56 misregulation of gene expression and significant growth defects, with Δ*hns* strains viable only in
57 combination with mutations in genes such as *rpoS* (the stationary-phase sigma factor) or *phoP* (a
58 two-component system response regulator) [16,18–20]. This contrasts with non-pathogenic
59 *Escherichia coli* (*E. coli*), where *hns* is non-essential, implicating the misexpression of virulence
60 genes as the basis for *hns* essentiality in STm [21,22]. Multiple virulence regulons are
61 derepressed in STm Δ*hns* strains, and deletion of the virulence regulator *ssrA* partially rescues
62 the growth defect of the Δ*hns* strain, demonstrating the contribution of H-NS-mediated repression
63 of virulence genes to STm fitness [16]. While H-NS ensures tight repression of virulence genes
64 under non-inducing conditions, this repression must be rapidly relieved in host environments. Host
65 environmental cues, such as changes in osmolarity, pH, and ion concentrations, activate
66 response regulators that displace H-NS from the promoters of virulence genes, enabling RNA
67 polymerase recruitment and transcription [23–25]. Therefore, optimal virulence gene regulation

depends on the coordinated interplay between H-NS-mediated repression and response regulator activity.

The interaction between H-NS-mediated repression and response regulator activity in virulence gene expression has been characterized primarily at the population level. However, single-cell studies reveal that virulence gene expression is highly heterogeneous in STm, even under uniform inducing conditions. This non-genetic variation, referred to as phenotypic heterogeneity, arises primarily from stochastic gene expression [26,27]. Generating distinct subpopulations of virulence-expressing and non-expressing bacteria enables bet-hedging or division-of-labor strategies that improve survival in hostile host environments [7,28]. In STm, phenotypic heterogeneity is associated with two major virulence regulons encoded in *Salmonella* Pathogenicity Islands 1 and 2 (SPI-1 and SPI-2) [29]. Expression of SPI-1, which is required for invasion of the intestinal epithelium, is bistable and incurs a fitness cost [5,30–32]. Both SPI-1(+) and SPI-1(-) subpopulations are required for a productive infection *in vivo*, and perturbing this ratio impairs infection outcomes. Expression of SPI-2, which is required for survival and replication within host cells, is bimodal and probabilistically tuned to the strength of intracellular-like signals, including pH and magnesium concentration, *in vitro* [31,33–38]. SPI-2 expression is heterogeneous within macrophages, with SPI-2(+) cells associated with anti-inflammatory gene expression profiles [39]. While the significance of phenotypic heterogeneity in STm virulence gene expression is well established, whether the relief of H-NS-mediated repression of virulence genes contributes to this cell-to-cell variation remains unknown.

While the role of H-NS in virulence gene expression heterogeneity remains unclear, it is well established that H-NS shapes pathogen evolution through its role as a global regulator of virulence gene expression [11,40,41]. H-NS-mediated repression is essential for maintaining virulence genes in the STm genome. Loss of *hns* causes growth defects that can be compensated by mutations in SPI-1 or SPI-2 genes, demonstrating that H-NS-mediated repression prevents fitness costs from the misexpression of virulence genes [16,40]. While the integration of virulence gene regulation with H-NS-mediated repression has enabled STm to maintain virulence genes and colonize diverse host environments, it may also act to constrain adaptive evolution. As a global regulator controlling the expression of hundreds of genes, H-NS may limit which genetic changes are beneficial as STm adapts to host environments. Understanding how H-NS impacts pathogen adaptation to intracellular environments may reveal how evolutionary constraints on this conserved global repressor shaped STm evolution in this critical host niche.

100 Here, we identify an H-NS DBD mutant strain of STm and use it to investigate how this global
101 repressor regulates heterogeneity in virulence gene expression and constrains adaptation to
102 intracellular-like conditions *in vitro*. By measuring virulence gene expression in individual bacteria,
103 we find that reduced H-NS repression increases the fraction of virulence gene expressing cells
104 without eliminating bimodality, and that this enhances epithelial cell infection. Using experimental
105 evolution, we demonstrate that while both wild-type and mutant populations converge on
106 disrupting virulence gene regulation to improve fitness in intracellular-like conditions, the *hns*
107 genotype constrains the mutational paths available for adaptation. These results suggest that H-
108 NS contributes to optimal virulence gene repression by setting activation thresholds in individual
109 cells, and that strong purifying selection on this global repressor limits evolutionary adaptive
110 strategies available to STm under intracellular-like conditions.

111 **RESULTS**

112 **Identification of a *Salmonella* strain with a mutation in the H-NS DNA-binding domain**

113 While investigating the growth of STm in SPI-2-inducing conditions (MgM-MES) *in vitro*, we
114 identified a strain with impaired growth compared to the wild-type (WT), while its growth in non-
115 inducing conditions (M9/Glc/CAA) was unaffected (Figure 1A). Quantification of growth metrics
116 confirmed that this mutant (MUT) strain had a significantly increased lag time and a reduced
117 maximum growth rate compared to the WT strain in MgM-MES (Figure 1A). To determine whether
118 this impaired growth was generalizable to other virulence-inducing conditions, we cultured the
119 strains in media used to induce the SPI-1 virulence regulon (LB High Salt: LB-HS) and found
120 growth was comparable between the two strains (Figure S1A). MgM-MES not only induces SPI-
121 2 but also imposes several stressors on the bacteria, including magnesium restriction, nutrient
122 limitation, and acidic pH. To test whether stress conditions were sufficient to elicit a growth defect
123 in the MUT strain, we measured growth in a nutrient-limited condition (M9/Glc without casamino
124 acids) (Figure S1A). The MUT strain showed impaired growth in M9/Glc compared to the WT
125 strain, with significant changes in lag time and maximum growth rate. Together, these data
126 demonstrate that the MUT strain has context-specific growth defects, with impaired growth in SPI-
127 2-inducing and nutrient-limiting media conditions.

128 To identify the genetic basis for this context-specific growth defect, we performed whole genome
129 sequencing on the WT and MUT strains. We identified a single missense mutation (a328g
130 [T110A]) in the DNA-binding domain (DBD) of *hns* (Figures 1B, S1B). The H-NS DBD is highly
131 conserved across enteric bacteria, with Thr110 completely conserved (Figure 1B) [42,43]. Several
132 other genetic changes were identified in the MUT strain (Figure S1B, Table S1). However, these

133 changes were located in either intergenic regions, a pseudogene, or in regions coding for
134 hypothetical proteins, and were therefore considered unlikely to cause the impaired growth of the
135 MUT strain. In STm, *hns* null mutations are viable only when accompanied by mutations in *rpoS*
136 or *phoP* [16,18,20]; therefore, this suggests that T110A is a hypomorphic mutation that impairs
137 but does not abolish H-NS repression. As such, the T110A strain is a unique tool to quantitatively
138 assess how altered H-NS repression affects virulence gene expression in individual bacteria.

139 **H-NS T110A has reduced DNA-binding affinity**

140 Based on the location of the T110A mutation in the highly conserved H-NS DNA-binding domain
141 and the T110A strain's growth defects, we hypothesized that the T110A mutation reduces H-NS
142 DNA-binding affinity. To assess how the T110A mutation might alter protein structure, we used
143 an NMR-resolved structure of the H-NS WT DBD from STm (PDB: 2L93) (Figure 2A) [15]. Two
144 consequences of the T110A mutation that could negatively impact DNA binding were apparent.
145 First, in the WT structure, Thr110 uses a side chain hydroxyl to form a polar interaction with
146 Gln112, a residue in the QGR motif. This motif mediates direct contacts between H-NS and the
147 DNA minor groove [15,44]. The substitution of Thr110 with alanine eliminates the side chain
148 hydroxyl and replaces it with a methyl group, resulting in the loss of the stabilizing hydrogen bond
149 between residues 110 and 112. Removing this polar interaction could destabilize the QGR motif
150 and reduce H-NS DNA-binding affinity. Second, the T110A mutation alters van der Waals forces.
151 In H-NS T110A, an interaction between Thr110 and Trp109 is lost, and a new interaction between
152 Ala110 and Lys96 is gained. The Thr110 - Trp109 interaction likely anchors the polar bond
153 between Trp109 and Gln112 to stabilize the QGR motif. This structural analysis confirms that
154 Thr110 is a critical residue in the H-NS DBD and suggests that the T110A mutation disrupts key
155 interactions in the DBD that are important for proper positioning of the QGR motif.

156 Next, to test whether the T110A mutation reduces H-NS DNA-binding affinity, we performed
157 electrophoretic mobility shift assays (EMSAs). We expressed and purified C-terminal 6xHis-
158 tagged full-length H-NS WT and T110A in *E. coli* using polyethyleneimine (to remove DNA), nickel
159 affinity chromatography, and size exclusion chromatography (Figures 2B, S2A-B). We selected a
160 region in the *ssrAB* promoter as the DNA probe because *ssrAB* is part of the SPI-2 virulence
161 regulon, is a known H-NS target, and this promoter region has been previously validated in H-NS
162 EMSAs (Figure S2C) [24,45,46]. As predicted from the structural analysis, H-NS T110A retained
163 DNA-binding capacity but had reduced affinity compared to H-NS WT (Figures 2C, S2D).
164 Although there was some variation between replicates, the reduced affinity of H-NS T110A for
165 DNA was reproducible. Free DNA probe was fully depleted between 750-950 nM for H-NS WT

166 compared to 1500-2000 nM for H-NS T110A. Quantification of binding and fitting to the Hill
167 equation confirmed that the average K_D for H-NS T110A (927.95 ± 133.98 nM) was higher than
168 for H-NS WT (635.65 ± 86.13 nM) (Figures 2C, S2E). These results demonstrate that the T110A
169 mutation impairs H-NS function by reducing DNA-binding affinity, consistent with findings for *E.*
170 *coli* H-NS DBD mutants [47,48].

171 **H-NS T110A alters features of virulence gene expression heterogeneity while preserving**
172 **bimodality**

173 Virulence gene expression in *Salmonella* is heterogeneous, with only a subset of cells activating
174 expression even under uniform virulence-inducing conditions [5,30–33,37,38]. H-NS plays a
175 critical role in repressing virulence genes in non-inducing conditions [16,18]; however, the extent
176 to which H-NS-mediated repression contributes to heterogeneity in virulence gene expression
177 remains unclear. The T110A strain provided a tool to investigate this by allowing a direct
178 comparison of single-cell virulence gene expression between strains with intact (WT) and
179 impaired (T110A) H-NS-mediated repression.

180 Bimodality in virulence gene expression typically arises from stochastic gene expression and
181 feedback in the gene regulatory network, generating subpopulations of responders and non-
182 responders [49–52]. However, virulence gene expression also requires the cognate response
183 regulators to displace H-NS from virulence gene promoters, allowing RNA polymerase
184 recruitment and transcription [16,18,23–25]. We hypothesized that if H-NS-mediated repression
185 contributes to heterogeneity in virulence gene expression, reduced H-NS DNA-binding affinity in
186 the T110A strain could affect this heterogeneity in several distinct ways, which can be
187 distinguished at the single-cell level (Figure 3A). For instance, in the T110A strain 1) the response
188 could be faster if H-NS is displaced more easily, 2) the fraction of responders could increase if H-
189 NS displacement is a limiting step in expression, or 3) the amplitude of expression could increase
190 if H-NS rebinding limits transcriptional output. Comparing virulence gene expression between H-
191 NS WT and T110A strains enabled us to determine whether H-NS-mediated repression
192 contributes to heterogeneity in virulence gene expression.

193 Given the impaired growth of the T110A strain in SPI-2-inducing media (MgM-MES, Figure 1A),
194 we first examined whether the mutation altered SPI-2 virulence gene expression patterns. To
195 measure SPI-2 transcriptional activity in individual bacteria, we used a previously described SPI-
196 2 transcriptional reporter consisting of the *ssaG* promoter (a promoter upstream of the primary
197 SPI-2 structural operon) fused upstream of a destabilized sfGFP (sfGFP-LVA) [33]. The reporter
198 plasmid also constitutively expresses mRuby2 for cell identification by flow cytometry. In the WT

199 strain grown in MgM-MES, SPI-2 reporter expression is bimodal, with bacteria progressively
200 switching into the SPI-2 ON state over several hours [33]. We compared SPI-2 reporter
201 expression between the WT and T110A strains in either SPI-2-inducing (MgM-MES (Glycerol)) or
202 non-inducing (M9/Glc/CAA) media after 2 and 4 hours of growth. In SPI-2-inducing media, the
203 T110A strain maintained bimodal SPI-2 reporter expression with distinct ON and OFF populations
204 (Figure 3B). We next evaluated whether any of the three features of response heterogeneity
205 (response timing, fraction of responders, and response amplitude) differed between the strains.
206 To evaluate response timing and the fraction of responders, we compared the fraction of GFP(+)
207 cells over time. At both 2 and 4 hours in SPI-2-inducing media, the T110A strain consistently had
208 a greater fraction of responders than the WT strain (Figure 3B, Table S2, 5/5 replicates, sign test,
209 p=0.0312). The increase in the fraction of GFP(+) cells at 2 hours, when cells first begin to express
210 the SPI-2 reporter [33], indicates that SPI-2 reporter expression is faster in the T110A strain. To
211 determine whether the increase in responder fraction over time in the T110A strain was a result
212 of its slower growth rate in MgM-MES and protein accumulation, we substituted glucose for
213 glycerol to increase the growth rate. At 4hrs, faster growth decreased the fraction of responders
214 in the WT but not in the T110A strain, indicating that differences in growth rate do not fully explain
215 the increase in responders in the T110A strain (Figure 3B, Figure S3A). Next, we evaluated the
216 amplitude of the SPI-2 reporter response and found it was generally similar between the two
217 strains, with only a modest increase in the mean fluorescence intensity (MFI) of the T110A GFP(-
218) subpopulation at 4 hours, which may result from slower growth (Figure S3B). As expected, in
219 non-inducing conditions, the SPI-2 reporter remained OFF in both strains (Figure S3C), indicating
220 that reduced H-NS DNA-binding affinity alone is insufficient to trigger reporter expression in the
221 absence of activated response regulators. Together, these data indicate that reduced H-NS DNA-
222 binding affinity in the T110A strain does not abolish the bimodal SPI-2 response but increases
223 the response rate and the fraction of responders.

224 Unlike SPI-2, SPI-1 expression imposes clear fitness costs, including a reduced growth rate that
225 is associated with increased antibiotic resistance [5,30]. In addition, the ratio of SPI-1(+) to SPI-
226 1(-) cells is a critical feature of the system *in vivo*. Mutations that decrease the fraction of SPI-1(-
227) cells lead to the emergence of genetically avirulent cells and limit infection [32]. The fitness cost
228 of SPI-1 expression together with the constraint on the responder fraction suggests that SPI-1
229 expression may be particularly sensitive to perturbations in H-NS-mediated repression. We
230 therefore hypothesized that reduced H-NS DNA-binding affinity in the T110A strain would
231 increase the fraction of SPI-1(+) cells.

232 To test this, we generated a SPI-1 transcriptional reporter consisting of the *invF* promoter (a SPI-
233 1 response regulator) fused upstream of sfGFP, with constitutive mRuby2 expression for cell
234 identification by flow cytometry. Similar plasmid-based reporters have been used in other studies
235 to examine cell-to-cell variation in the SPI-1 response [53]. To test whether H-NS-mediated
236 repression impacts the fraction of responders, we examined reporter expression in SPI-1-inducing
237 conditions (LB High Salt) and quantified the fraction of responders at 3, 4, and 5 hours by flow
238 cytometry (Figure 3C). The T110A strain maintained bimodal expression of the SPI-1 reporter but
239 had a higher fraction of responders than the WT, and this difference remained stable over time
240 (Figure 3C, Table S2). The MFI of the SPI-1(-) and SPI-1(+) subpopulations were similar between
241 the strains (Figure S3D). As expected, in non-inducing media (LB), the SPI-1 reporter remained
242 OFF in the WT strain (Figures 3C, S3E). In contrast, the T110A strain showed a small but
243 consistent increase in the fraction of SPI-1(+) cells above the WT level that remained stable over
244 time. Neither strain had reporter expression prior to the start of the assay, indicating this difference
245 arose during the experimental growth period (Figure S3E). Since WT and T110A strains grow
246 similarly in LB (Figure S1A), growth differences are not responsible for this increase in GFP(+)
247 cells. It is possible that the use of a stable fluorescent protein results in GFP accumulation as
248 cells enter stationary phase, potentially amplifying small differences in leaky expression caused
249 by reduced H-NS repression in the T110A strain.

250 Both SPI-1 and SPI-2 responses remain robustly bimodal despite impaired H-NS function,
251 demonstrating that H-NS does not determine whether virulence gene expression is
252 heterogeneous. Instead, H-NS-mediated repression affects features of virulence heterogeneity,
253 specifically the timing of the response and the fraction of responding cells (Figure 3D). The T110A
254 mutation had a large effect on SPI-1 heterogeneity, suggesting that the activation threshold for
255 SPI-1 virulence gene expression is sensitive to changes in H-NS DNA binding affinity (Figure 3D).
256 In the T110A strain, lowering the SPI-1 activation threshold allows more cells to become SPI-1(+),
257 while other known regulatory mechanisms maintain bimodality.

258 **Reduced H-NS function enhances *Salmonella* infection of epithelial cells**

259 Expression of the SPI-1 regulon drives production of a T3SS required for invasion of epithelial
260 cells [29,54,55]. Given the increased fraction of SPI-1(+) cells in the T110A strain, we asked
261 whether this translates to enhanced epithelial cell infection. While the SPI-1 reporter reflects *invF*
262 transcriptional activation, numerous subsequent steps are required for T3SS assembly and
263 function [56]. In addition, a recent study of *E. coli* flagellar gene regulation revealed that distal
264 genes can exhibit variable expression despite homogeneous expression of a proximal regulator

265 [57]. As a result, the increased fraction of SPI-1 reporter ON cells in the T110A strain might not
266 necessarily result in increased invasion capacity. Invasion can also be impacted by the ratio of
267 SPI-1(+) to SPI-1(-) cells. The presence of both subpopulations was shown to maximize the
268 invasion frequency of epithelial cells in culture, while a SPI-1(+) only subpopulation showed
269 reduced invasion frequency [58]. To test whether the increased fraction of SPI-1(+) cells in the
270 T110A strain increased epithelial cell infection, we infected HeLa cells with H-NS WT and T110A
271 strains constitutively expressing mRuby2 and quantified infection using microscopy. We found the
272 T110A strain increased the frequency of infected HeLa cells compared to WT across all
273 multiplicities of infections (MOIs) tested (Figure 3E, Table S2). We further characterized infection
274 by quantifying the fraction of infected HeLa cells containing multiple bacteria, using area and total
275 intensity of segmented bacterial objects to distinguish between single and multi-bacteria infection
276 events. At higher MOIs (50, 100), where multi-bacteria infection events are more likely to occur,
277 the T110A strain showed an increased frequency of such events compared to the WT, as well as
278 more bacteria per cell, as evidenced by greater area and total intensity of segmented bacteria
279 (Figure 3E). Differences in bacterial replication cannot account for this effect, as bacteria were
280 quantified shortly after infection, before intracellular replication had begun. Instead, the increase
281 in multi-bacteria infection events in the T110A strain likely results from both the increased fraction
282 of SPI-1(+) cells and enhanced membrane ruffling of epithelial cells. SPI-1(+) cells secrete
283 effector proteins that hijack the host cytoskeleton and induce membrane ruffling, which has been
284 shown to stimulate uptake of SPI-1(+) and nearby SPI-1(-) cells [59]. Together, these results
285 demonstrate that reduced H-NS DNA binding affinity directly affects epithelial cell infection.

286 ***hns* genotype restricts evolutionary adaptive strategies in SPI-2 inducing environments**

287 The H-NS DBD is highly conserved across enteric bacteria (Figure 1B), indicating strong selection
288 against mutations in this region. Mutations in global regulators such as H-NS may be particularly
289 deleterious as they can have wide-ranging effects - the T110A strain has both fitness defects in
290 SPI-2-inducing and nutrient-limited media (Figures 1A, S1A), as well as altered virulence gene
291 expression (Figures 3B-C). We hypothesized that the *hns* genotype may therefore alter which
292 mutations provide fitness benefits during adaptation to SPI-2-inducing conditions, thereby
293 constraining evolutionary trajectories. In the T110A background, impaired H-NS repression
294 potentially favors mutations that reduce activation of target genes, such as the virulence genes
295 which are misregulated in this strain. Additionally, selection may favor reversion of the T110A
296 mutation or require compensatory mutations elsewhere in the genome. In contrast, H-NS
297 repression is intact in the WT strain, which may favor a distinct set of adaptive mutations.

298 Comparing evolutionary trajectories between the H-NS WT and T110A strains would reveal
299 whether the starting *hns* genotype constrains the paths available for adaptation. In addition,
300 comparing the magnitude of fitness gains between the strains could indicate whether the WT
301 strain, in which H-NS repression of target genes has been optimized over evolutionary timescales,
302 has limited capacity for fitness gains relative to the T110A strain, in which H-NS function is
303 impaired.

304 To test this hypothesis, we performed experimental evolution by serially passaging six
305 independent cultures of each strain in SPI-2-inducing media (MgM-MES) for 30 days (Figure 4A)
306 and compared growth metrics, genomic changes, and virulence gene expression. We chose
307 MgM-MES because the T110A strain has a severe fitness defect and altered SPI-2 gene
308 expression in this media. Although WT grows better than T110A in MgM-MES, its growth is still
309 reduced compared to replete media, suggesting there are still opportunities for adaptation. WT
310 and T110A evolved clones displayed distinct growth dynamics (Figures 4A, S4A). At day 5, the
311 WT clones showed no improvement compared to the ancestral WT strain. In contrast, five of six
312 T110A strains had improved fitness and surpassed even the ancestral WT strain, with variable
313 changes in lag time, maximum growth rate, and maximum OD_{600}. By day 30, all WT clones had
314 increased fitness relative to the ancestral WT strain with improvements in all growth metrics,
315 although the magnitude of improvement varied between clones. The T110A clones maintained
316 their improved fitness over the ancestral WT strain at day 30. The differences in the timing of
317 fitness improvements (faster adaptation for T110A) suggest that distinct mutational trajectories
318 occur in each *hns* genotype and that *hns* DBD mutants are genetically unstable, similar to Δ*hns*
319 strains [40].

320 To identify strain-specific adaptive mutations, we performed whole-genome sequencing on all day
321 30 evolved clones (Figures 4B, S4B). Based on hierarchical clustering of the acquired mutations,
322 WT and T110A clones clustered separately, except for T110A clone 4, which was grouped with
323 the WT clones. Despite the fitness cost of the T110A mutation in MgM-MES, none of the T110A
324 clones reverted to wild type. Instead, all T110A clones acquired compensatory mutations in at
325 least one of *ssrA* (a sensor kinase that activates the SPI-2 master regulator SsrB), *phoQ* (a sensor
326 kinase that activates SPI-2 in response to acidic pH and limited magnesium), or *rpoS* [20,60–64].
327 The prevalence of *rpoS* mutations is consistent both with H-NS promoting RpoS degradation and
328 the viability of STm Δ*hns* strains often depending on compensatory mutations in *rpoS* [16,18,65].
329 One T110A clone (clone 3) acquired a mutation in *mutS*, a mismatch repair gene, resulting in
330 numerous additional mutations [66]. In contrast to the T110A clones, all WT clones acquired

331 mutations in genes related to the PhoPQ two-component system. Five clones carried mutations
332 in the sensor kinase *phoQ*, while one carried a mutation in *proQ*, an RNA-binding protein that
333 positively regulates the PhoP regulon [67,68]. While mutations in both WT and T110A clones
334 target the SPI-2 gene regulatory network (GRN), they occur in distinct nodes of the network.
335 Sequencing of three day 5 T110A clones revealed few mutations, consistent with these
336 populations likely being a mixture of cells carrying different mutations that had yet to become fixed
337 in the population (Figure S4B).

338 To assess whether these mutations in the SPI-2 GRN altered virulence gene expression, we
339 measured SPI-2 reporter expression in two representative day 30 clones from each background
340 (WT clones 3 and 5, T110A clones 2 and 5). After 4 hours in MgM-MES, all four clones showed
341 negligible GFP(+) cells by flow cytometry (Figures 4C, S4C). In three of the clones, the small
342 fraction of GFP(+) cells had intensity measurements similar to those of rare cells in the GFP(-)
343 control strain labeled as GFP(+), confirming that these cells are unlikely to be SPI-2 responders
344 (Figure S4C). Only T110A clone 2 had GFP(+) cells of similar intensity to the ancestral strains,
345 indicating that this clone retained SPI-2 activity, albeit in a much decreased fraction of cells.

346 Overall, the genomic changes observed in the evolved clones confirm that distinct adaptive
347 mutations occur in each *hns* genotype, suggesting that T110A clones must compensate for the
348 broader effects of H-NS target gene misregulation. Together, these results reveal how
349 evolutionary constraints on a highly conserved global regulator impact pathogen adaptation to
350 intracellular-like environments.

351 **DISCUSSION**

352 Here, we characterized an STm strain with a mutation (T110A) in the H-NS DBD to assess the
353 contribution of H-NS-mediated repression to virulence gene expression heterogeneity and
354 pathogen adaptation to intracellular-like environments. Biochemical characterization confirmed
355 the T110A mutation reduced H-NS DNA-binding affinity *in vitro*. Using SPI-1 and SPI-2
356 transcriptional reporters, we found that this reduced H-NS DNA-binding affinity increased the
357 fraction of responding cells while preserving bimodal expression of the virulence reporters. The
358 increased fraction of SPI-1(+) cells in the T110A strain had functional consequences, resulting in
359 increased infection of epithelial cells *in vitro*. Finally, using experimental evolution we demonstrate
360 that *hns* genotype constrains adaptive mutations to intracellular-like conditions, with distinct
361 mutations associated with fitness gains in each strain. Together, our findings establish that the
362 global repressor H-NS contributes to virulence gene expression heterogeneity by modifying

363 virulence activation thresholds in individual bacteria, while strong purifying selection on the H-NS
364 DBD restricts the mutational paths available during adaptation to intracellular-like environments.

365 Optimal H-NS-mediated repression of virulence genes requires both tight silencing in non-
366 inducing environments and the rapid relief of this silencing upon exposure to inducing conditions.
367 The critical role of H-NS in silencing virulence gene expression in non-inducing environments has
368 been well-established using Δ*hns* strains, while elegant biochemical studies have characterized
369 the role of response regulators in displacing H-NS from virulence gene promoters to enable
370 expression [16,18,23,24,40]. However, whether H-NS-mediated repression modulates
371 heterogeneity in virulence gene expression in inducing conditions has remained unclear for
372 several reasons. First, evaluating the role of a global regulator like H-NS in virulence
373 heterogeneity is challenging because Δ*hns* strains cause widespread gene dysregulation and
374 severe growth defects even in rich media, rapidly selecting for compensatory mutations that
375 confound interpretation of the contribution of H-NS to any phenotype [16,18,40]. Second, in Δ*hns*
376 strains, several STm virulence regulons are broadly expressed in non-inducing environments,
377 precluding analysis of how relief of H-NS repression impacts virulence heterogeneity in inducing
378 conditions [16,18]. The H-NS T110A mutant overcomes both challenges and, as such, is ideally
379 suited to evaluate how impaired H-NS function impacts virulence gene expression heterogeneity.
380 In non-inducing conditions, the T110A strain grows normally, limiting selective pressure for
381 compensatory mutations, and maintains virulence gene repression, enabling the role of H-NS in
382 virulence gene activation to be directly evaluated.

383 The preservation of bimodality in both SPI-1 and SPI-2 responses in the T110A strain
384 demonstrates that H-NS itself does not determine whether heterogeneity occurs, but instead it
385 modifies features of the virulence response at the single-cell level. For both SPI-1 and SPI-2, the
386 fraction of responders is the feature most affected by reduced H-NS DNA-binding affinity (Figure
387 3). While the activation of response regulators sets an activation threshold that individual bacteria
388 must exceed to express virulence genes, our results indicate that H-NS repression can adjust this
389 threshold, at least in a subset of cells. Two models to explain the increase in the fraction of
390 virulence responders in the T110A strain are: 1) response regulator levels vary continuously
391 across the population, and in certain bacteria these levels are insufficient to displace H-NS WT
392 but sufficient to displace the reduced affinity H-NS T110A, or 2) H-NS repression of virulence
393 genes varies between individual bacteria, such that weakening H-NS repression shifts only a
394 subset of cells past the activation threshold. These models make distinct, testable predictions,
395 although testing them will require technically challenging measurements such as determining the

396 relationship between levels of response regulators and virulence gene expression in individual
397 bacteria or quantifying variation in H-NS deposition at virulence gene promoters in single bacteria.

398 STm has evolved to navigate fluctuating host environments and adjust virulence gene expression
399 accordingly [3,4]. As such, virulence gene expression is a dynamic process in which the
400 coordinated interplay between H-NS and response regulators is ongoing as the pathogen cycles
401 between modes of virulence gene activation and repression based on environmental cues.
402 Examining virulence responses in single cells over time has revealed critical features of the SPI-
403 2 response, including switch-like activation and heterogeneity in response timing [33]. An
404 important future extension of our findings will be to examine virulence gene expression over time
405 in individual bacteria with either intact or impaired H-NS repression, both *in vitro* and in host cells.
406 The H-NS T110A mutation may have consequences that extend beyond the fraction of virulence
407 responders. For instance, the WT and T110A strains could differ in the trajectory of the virulence
408 response, the stability of expression across generations, or the reversibility of the response as
409 cells transition to new environments, all processes that involve either the relief or reestablishment
410 of H-NS repression. Such studies will be critical to gain mechanistic insight into how H-NS
411 repression of virulence genes has been optimized over evolutionary time.

412 H-NS repression plays a critical role in the maintenance of virulence genes and thus enables
413 *Salmonella* colonization of diverse host environmental niches [16,18,29,36,40,69]. However,
414 whether H-NS itself, as a result of its highly conserved DBD, constrains mutations during
415 adaptation to new host environments was unclear. Combining experimental evolution with the
416 T110A strain enabled us to demonstrate that evolutionary trajectories in SPI-2 inducing conditions
417 differed in several key ways depending on the starting *hns* regulatory state. While both WT and
418 T110A strains converged on disrupting the SPI-2 regulatory network, mutations arose in different
419 nodes in the network depending on the starting *hns* genotype. T110A clones likely selected for
420 mutations that simultaneously improve fitness and compensate for baseline gene expression
421 dysregulation, whereas WT clones, lacking this dysregulation could select for a distinct set of
422 mutations. Revertants restoring WT H-NS were never observed, suggesting that if compensatory
423 mutations restore fitness, reversion is unlikely, consistent with simulations of reversion frequency
424 in bacteria [70]. Differences in the dynamics of adaptation revealed that the context-specific
425 growth defects of the T110A strain rapidly select for compensatory mutations in SPI-2 inducing
426 conditions, consistent with strong purifying selection on the H-NS DBD (Figures 1, 4). Finally, in
427 both *hns* genotypes, adaptation came at a cost, the loss of SPI-2 inducing capacity. This indicates
428 a tradeoff between fitness and maintenance of intact virulence gene regulation and suggests that

429 SPI-2 expression incurs a fitness cost, at least under prolonged exposure to inducing conditions.
430 Although technically challenging to implement, future experimental evolution approaches should
431 incorporate periodic selection for functional SPI-2 to reveal whether bacterial populations can
432 simultaneously optimize growth and maintain inducible virulence gene regulation, or whether this
433 is a fundamental constraint that limits pathogen adaptation.

434 In summary, we find that evolutionary constraints on the global regulator H-NS restrict both
435 heterogeneity in virulence gene expression and pathogen adaptation to intracellular-like
436 environments. Our findings demonstrate that optimization of H-NS repression extends beyond
437 tight silencing of virulence genes in non-inducing environments to include rapid and
438 heterogeneous activation upon exposure to intracellular-like conditions, and that H-NS DBD
439 mutants will be a valuable resource to further dissect this process.

440 **ACKNOWLEDGEMENTS** We thank members of the Lane lab for discussions and valuable
441 feedback on the manuscript. We thank members of the Blythe, Brickner, Horvath, Lackner,
442 Mondragón, and Weiss labs for advice, reagents, and technical assistance with protein
443 purification and EMSAs. We thank the Robert H. Lurie Comprehensive Cancer Center Flow
444 Cytometry Core Facility of Northwestern University and the Single Cell Genomics Core for flow
445 cytometry training and equipment. The Lurie Cancer Center is supported in part by an NCI Cancer
446 Center Support Grant #P30 CA060553. We thank the Northwestern Center for Synthetic Biology
447 Biofoundry for training and use of the AKTA Avant 25 for SEC. UCSF ChimeraX was developed
448 by the Resource for Biocomputing, Visualization, and Informatics at the University of California,
449 San Francisco, with support from National Institutes of Health R01-GM129325 and the Office of
450 Cyber Infrastructure and Computational Biology, National Institute of Allergy and Infectious
451 Diseases. We acknowledge our funding sources: NIH Cellular and Molecular Basis of Disease
452 Training Program award to MRS (NIH T32 GM008061) and a Northwestern Weinberg College of
453 Arts and Sciences Baker Faculty Research Program award to K.L.

454 **AUTHOR CONTRIBUTIONS**

455 Conceptualization: MS, KL. Data curation: LM, DK, KL. Formal analysis: LM, DK, MS, MB, JZ,
456 KL. Funding Acquisition: MS, KL. Investigation: LM, DK, MS, MB, JZ, KL. Methodology: LM, MS,
457 KL. Project Administration: KL. Resources: MS, KL. Supervision: KL. Validation: KL. Visualization:
458 LM, DK, MS, KL. Writing - Original Draft Preparation: LM, MS, KL.

459 **METHODS**

460 Essential reagents and catalog numbers are listed in Table S3.

461 ***Salmonella* strains**

462 The *Salmonella enterica* serovar Typhimurium 14028 strain used as wild type (WT) was a gift
463 from the laboratory of Michael McClelland. The *hns* mutant strain was isolated from a preceptrol
464 freeze-dried stock of *Salmonella enterica* serovar Typhimurium 14028 obtained from ATCC
465 (ATCC 14028). The strain was rehydrated and streaked on nutrient agar according to ATCC
466 protocols. Colonies from the initial streak varied in morphology, and several appeared mucoid.
467 Individual colonies were restreaked onto LB agar plates and glycerol stocks were prepared. One
468 glycerol stock was used for all experiments and is referred to as the *hns* mutant or T110A strain
469 throughout.

470 ***Salmonella* Cell Culture**

471 Bacterial strains were streaked from glycerol stocks onto LB agar containing appropriate selective
472 antibiotics and incubated overnight at 37˚C. Plates were used for experiments within one week
473 and culture growth kept to a minimum to avoid issues of genomic instability associated with *hns*
474 mutant strains [40]. Cultures were grown at 37˚C with shaking (250 rpm). Growth media
475 compositions: LB-Lennox (LB): NaCl 5g/L; LB-Miller (LB High Salt): NaCl 10g/L (SPI-1 inducing
476 media); M9/Glc/CAA: 1x M9 salts, 0.1mM $CaCl_2$, 2mM $MgSO_4$, 0.4% glucose, 0.2% casamino
477 acids; M9/Glc: 1x M9 salts, 0.1mM $CaCl_2$, 2mM $MgSO_4$, 0.4% glucose; MgM-MES (SPI-2 inducing
478 media): 5mM KCl, 7.5mM $(NH_4)_2SO_4$, 0.5mM K_2SO_4, 1mM KH_2PO_4, 170mM 2-(N-
479 morpholino)ethanesulphonic acid hydrate (pH adjusted to 5.0 with NaOH), 0.1% casamino acids,
480 38mM glycerol, 8μM $MgCl_2$ [71,72]. Where indicated, glycerol was replaced with 0.4% glucose.

481 **Plasmids, Cloning, and *Salmonella* Strain Generation**

482 All plasmids and strains generated in this study are listed in Table S4. Plasmids were assembled
483 using either Golden Gate Assembly with the EcoFlex library or Gibson assembly [73]. *E. coli* TG1
484 cells were used for all cloning steps. Plasmids were verified by Sanger sequencing or whole
485 plasmid sequencing.

486 *SPI-1 reporter plasmid (P_{invF}-sfGFP):* The *invF* promoter region (340 bp upstream of the start
487 codon plus 179 bp of the coding region) was previously described [53] and was amplified from
488 STm genomic DNA using PrimeSTAR Max DNA polymerase and cloned into a Golden Gate Level
489 0 promoter plasmid using Gibson assembly. A Level 1 single transcriptional unit (TU) plasmid
490 containing the promoter, ribosome binding site, open reading frame, and terminator was
491 assembled by Golden Gate Cloning. This plasmid was combined with a second TU expressing a
492 constitutive mRuby2 to generate the final Level 2 plasmid.

493 *SPI-2 reporter plasmid (PssaG-sfGFP-LVA) and constitutive mRuby2 plasmid (P_{SJM901}-mRuby2):*
494 These plasmids were generated using the same strategy and have been previously described
495 [33].

496 *Strain construction:* Electrocompetent cells were prepared using the mannitol-glycerol preparation
497 method [74]. Reporter plasmids were used to transform bacteria, and transformants were selected
498 on LB agar plates containing the appropriate antibiotic (see Table S4.2). WT strains containing
499 the SPI-2 reporter plasmid or the constitutive mRuby2 plasmid were previously generated [33].
500 Glycerol stocks were prepared by mixing 700µl overnight culture (grown in LB with appropriate
501 antibiotics) with 300µl of 50% w/v glycerol, vortexing, and storing at -80˚C.

502 **Mammalian Cell Culture**

503 HeLa cells from ATCC were maintained in DMEM supplemented with 10% FBS, 1x
504 Penicillin/Streptomycin, and 2mM GlutaMAX at 37˚C, 5% CO_2. Cell lines were not authenticated.

505 **Generation of Stable Cell Lines**

506 Lentivirus was produced in Lenti-X 293T cells using packaging plasmids psPAX2 (Addgene
507 #12260) and pMD2.g (Addgene #12259). HeLa cells were transduced with lentivirus expressing
508 H2B-miRFP670 and selected with hygromycin.

509 **Plate Reader Growth Assays and Analysis**

510 Single colonies were inoculated into the appropriate pre-culture medium (M9/Glc/CAA for
511 M9/Glc/CAA, M9/Glc, and MgM-MES plate reader samples and LB-Lennox for LB-Lennox and
512 LB-Miller plate reader samples) and grown shaking at 37˚C for 14-16 hours. Overnight cultures
513 were backdiluted to OD_{600} of 0.06 in 3 mL of the same media and grown shaking for 3 hours. Cells
514 were pelleted, washed twice in the plate reader media, and diluted to OD_{600} of 0.002. Three
515 technical replicates (150µl each) were added to a glass-bottom 96-well black plate. Plates were
516 sealed with breathable film, and a needle was used to pierce each well to ensure aeration.
517 Following a 30-minute equilibration in the plate reader (Tecan Spark) at 37˚C, OD_{600} was
518 measured at 5-minute intervals for 24 hours. Growth curve metrics were extracted using the
519 Omniplate software package [75]. Plots were generated using Seaborn and Matplotlib in Python
520 [76,77]. Statistical analyses were performed in Python (scipy and statsmodels) using unpaired t-
521 tests. Asterisks denoting significance level are indicated in the Figure legends.

522 **Whole Genome Sequencing (WGS) and Analysis**

523 Strains were streaked onto LB agar plates and incubated overnight at 37˚C. Single colonies were
524 inoculated into 3 mL LB and grown shaking overnight at 37˚C. Genomic DNA was isolated from
525 0.5-1 mL of culture using the Wizard(R) Genomic DNA purification kit (Promega) and eluted in
526 Tris pH 8.5. DNA samples were processed for Illumina whole-genome sequencing (200 Mbp
527 sequencing) by SeqCenter (https://www.seqcenter.com/).

528 Sequencing reads were analyzed using *breseq* [78]. FASTQ files were aligned to the STm 14028s
529 reference genome, including the chromosome (GenBank: CP001363.1) and plasmid (GenBank:
530 CP001362.1) sequence files. All samples were compared to the STm WT strain used in the lab.
531 The mutation heatmap (Figure 4B) was generated in R using the pheatmap package with binary
532 distance clustering (clustering_distance_cols = 'binary') and complete linkage (clustering_method
533 = 'complete'). A complete list of genetic changes for all WGS samples is reported in Table S1.

534 **Protein Sequence Alignment**

535 Protein sequences of H-NS homologs from Gram-negative enteric bacteria were retrieved from
536 UniProt. VicH, an H-NS-like protein from *Vibrio cholerae*, was also included [79]. Sequences were
537 aligned using Clustal Omega with output order set to match input order [80]. Alignments were
538 visualized using Jalview with color set to percent identity and conservation scores displayed [81].

539 **Protein Structure Analysis**

540 Structural analysis was performed in UCSF ChimeraX using the NMR-resolved structure of the
541 STm H-NS DNA-binding domain (PDB ID: 2L93) [15,82]. The T110A mutant model was generated
542 by substituting alanine for threonine at position 110 in the wild-type structure. Wild type and T110A
543 models were compared to evaluate local structural effects of the substitution around the QGR
544 motif. Hydrogen bonds were displayed, and van der Waals interactions were identified by
545 displaying contacts within 3.5 Å.

546 **Protein Expression and Purification**

547 Expression plasmids for H-NS WT and T110A were generated in the pET-28a backbone with a
548 C-terminal PreScission protease (PPX) cleavage site and 6xHis tag (Figure S2A). Expression
549 plasmids were used to transform competent *E. coli* BL21 (DE3) cells, and transformants were
550 selected on LB agar with kanamycin (50 µg/mL). Cultures were grown in LB-Lennox with
551 kanamycin to OD_{600} of 0.5, induced with 0.5 M isopropyl-beta-D-thiogalactopyranoside (IPTG),
552 and grown for 2 hours at 37°C with shaking (250 rpm). Cells were pelleted (14,000 rpm, 30
553 minutes, 4°C), resuspended in lysis buffer (20mM Tris-HCl pH 8, 150mM NaCl, 5% v/v glycerol,
554 2mM 1,4-dithiothreitol (DTT), 1mM phenylmethylsulfonyl fluoride (PMSF), 1x EDTA-free protease

555 inhibitor) and sonicated on ice (Branson, output control of 2.5%, 20% duty cycle, 5-second pulses
556 with 45-second rest intervals on ice). Lysates were clarified by centrifugation (14,000 rpm,
557 30 minutes, 4°C). All subsequent precipitation steps were performed at 4°C. DNA was precipitated
558 out of clarified lysates by adding polyethyleneimine (PEI; avg. MW 60 K) slow and drop-wise:
559 0.4% PEI in 150mM NaCl for H-NS WT, and 0.35% PEI in 1M NaCl for H-NS T110A. Samples
560 were incubated for 15 minutes with gentle stirring and then centrifuged (11,000*xg*, 15 minutes,
561 4°C). The supernatant was gently decanted into a beaker, and H-NS was salted out by slow
562 addition of powdered ammonium sulfate to 37% saturation. The solution was stirred gently
563 overnight, and precipitated H-NS was collected by centrifugation (15,000 rpm, 40 minutes, 4°C).
564 The H-NS precipitate was carefully resuspended in 10 mL of binding buffer (20mM Tris-HCl pH
565 8, 300mM NaCl, 20mM imidazole, 5mM β-mercaptoethanol). Samples were applied to pre-
566 equilibrated Ni-NTA agarose resin (Invitrogen) and incubated on ice with gentle rocking for 1 hour.
567 Resin was pelleted (800*xg,* 1 minute, 4°C), and the flow-through was discarded. To reduce non-
568 specific binding and disrupt remaining protein-DNA interactions, the resin was washed with wash
569 buffer (20mM Tris-HCl pH 8, 600mM NaCl, 50mM imidazole, 5mM β-mercaptoethanol) for 1 hour
570 on ice with gentle rocking, then pelleted (800*xg*, 1 minute, 4°C). Wash buffer was decanted, and
571 cleavage buffer was added (20mM Tris-HCl pH 8, 300mM NaCl, 5mM β-mercaptoethanol) along
572 with PreScission Protease (1µl per nmol H-NS). Samples were incubated on ice with gentle
573 rocking for 4 hours. Resin was pelleted (800*xg*, 1 minute, 4°C) and the H-NS-containing flow-
574 through was collected. Samples were concentrated using a 3kDa MWCO cutoff Ultra Centrifugal
575 Filter (Amicon) and subjected to size-exclusion chromatography (SEC) on a Superdex 75
576 Increase 10/300 GL column (Cytiva) equilibrated in SEC buffer (20 mM Tris-HCl pH 8.0, 300 mM
577 NaCl, 5% glycerol, 5 mM β-mercaptoethanol) and run at a flow rate of 0.8 mL/min on an ÄKTA
578 Avant 25 system (GE Healthcare) at Northwestern University's Biofoundry Core. Peak fractions
579 were analyzed by Coomassie-stained SDS–PAGE and UV–Vis spectrophotometry. Protein purity
580 was quantified from the Coomassie-stained gel using ImageJ [83] and determined to be ~90% for
581 H-NS WT and 99% for H-NS T110A. Absorbances at 260 nm and 280 nm were used to verify
582 protein concentration and absence of nucleic acids. A_{260}/A_{280} ratios for all samples were
583 approximately 0.6, consistent with minimal nucleic acid contamination. Samples were flash-frozen
584 in liquid nitrogen and stored at -80°C.

585 **Electrophoretic Mobility Shift Assays (EMSAs) and Analysis**

586 A region of the *ssrAB* promoter region was amplified from STm genomic DNA using PrimeSTAR
587 DNA Polymerase (Takara) with primers previously described (Figure S2C) [45]. PCR products

588 were purified (Zymo Research) and verified by gel electrophoresis and Sanger sequencing
589 (Azenta). WT and T110A H-NS proteins were exchanged into EMSA binding buffer (20mM Tris-
590 HCl pH 7.4, 4mM $MgCl_2$, 100mM NaCl, 1mM DTT) using 3kDa MWCO cutoff Ultra Centrifugal
591 Filters (Amicon). Binding reactions were assembled in 0.2 mL reaction tubes. Water, then EMSA
592 Binding Buffer was added to the desired volumes and mixed. Protein was added (0, 200, 350,
593 450, 550, 600, 650, 750, 850, 950nM, 1, 1.5, 2, 3μM) and gently mixed. In 30-second increments,
594 25ng DNA probe per reaction tube was added. Samples were incubated at room temperature for
595 30 minutes. Loading dye (40% glycerol, 0.25% bromophenol blue) was added, and samples were
596 loaded onto a 5% native Mini-PROTEAN TBE gel (Bio-Rad) in 30-second increments to maintain
597 consistent timing across reactions. Gels were run at 100V in 0.5x TBE buffer for 30 minutes,
598 stained with Sybr Safe (Invitrogen), and washed twice with 150 mL Milli-Q H_2O. Gels were imaged
599 on an Azure 600 (Azure Biosystems Inc.) with a 10-second exposure time.

600 Gels were quantified using ImageJ. Background subtraction was performed by measuring the
601 median intensity of four background regions and calculating the mean. Bound and unbound DNA
602 regions were defined for each lane on a gel using the ROI manager tool. The fraction bound was
603 calculated for each lane as: fraction bound = (bound) / (bound + unbound), and a min-max
604 normalization was performed. All calculations and non-linear regression fitting to the Hill equation
605 were performed using SciPy and Python.

606 **SPI-1 and SPI-2 Induction Assays**

607 *SPI-1 induction:* Single colonies were inoculated into 3 mL LB-Lennox with appropriate antibiotics
608 and grown shaking at 37°C for 14-16 hours. Overnight cultures (BD1) were back diluted to OD_{600}
609 of 0.06 in fresh LB-Lennox and grown shaking for 2.5 hours (BD2). Cultures were then back
610 diluted to an OD_{600} of 0.06 into 5 mL LB-Miller (SPI-1 inducing) or LB-Lennox (control). At the
611 indicated fixation timepoints, 600μl of culture was mixed with 200μl of 16% paraformaldehyde by
612 inversion and incubated at room temperature for 30 minutes. Fixed samples were washed three
613 times with 1 mL PBS before storing in 1 mL PBS at 4˚C. Samples were analyzed by flow cytometry
614 within one week of fixation.

615 *SPI-2 induction:* Single colonies were inoculated into 3 mL M9/Glc/CAA with appropriate
616 antibiotics and grown shaking at 37°C for 14-16 hours. Overnight cultures were back diluted 1:100
617 into 3 mL fresh M9/Glc/CAA and grown shaking for 4 hours. Cultures were then back diluted to
618 an OD_{600} of 0.02 in 5 mL of MgM-MES containing either glycerol or glucose. Samples were fixed
619 and stored as described for SPI-1 induction.

620 **Flow Cytometry and Analysis**

621 Fixed samples were diluted in PBS to achieve approximately 10,000 events per second or below.
622 Samples were analyzed on a BD LSRFortessa SORP Cell Analyzer with HTS (6-laser 18-
623 parameter). At least 50,000 mRuby2 positive events were captured per sample.

624 Data were analyzed using FlowJo v10.8.2. Forward scatter (FSC) and side scatter (SSC) gates
625 were drawn to capture the majority of events. All reporter strains constitutively express mRuby2;
626 therefore, mRuby2 positive gates were set using negative control samples (cells without the
627 mRuby2 plasmid) such that less than 0.05% of the negative control events were classified as
628 mRuby2 positive. mRuby2 positive events were downsampled to 50,000 using the FlowJo
629 Downsample plugin (V3.3.1) for all subsequent analyses. GFP-positive gates were set using a
630 GFP-negative control sample (strain with a promoterless GFP control plasmid). Statistics,
631 including mean fluorescence intensity (MFI) and percentage of GFP(-) and GFP(+) cells, were
632 exported from FlowJo. Plots were generated using Seaborn and Matplotlib in Python. Statistical
633 analyses were performed in Python (scipy and statsmodels). Comparisons of percent GFP(+)
634 cells between strains were analyzed using a linear mixed-effects model with strain, time and
635 media as factors and accounting for repeated measures from the same culture tube. Post-hoc
636 pairwise comparisons between WT and T110A strains within each media-time combination (SPI-
637 2 data: 4 total (2 media, 2 timepoints), SPI-1 data: 6 total (2 media, 3 timepoints)) were performed
638 using unpaired t-tests with p values corrected for multiple comparisons using the Holm-Sidak
639 method. Consistency in trends across replicates was assessed using the sign test. Asterisks
640 denoting significance level are indicated in the Figure legends.

641 **Fluorescence Microscopy**

642 HeLa cells were plated at 6,000 cells/well on fibronectin-coated (10µg/ml) 96-well glass bottom
643 plates one day prior to infection. Bacterial cultures were prepared as described in the SPI-1
644 induction assays: Single colonies were inoculated into 3mL LB-Lennox with appropriate antibiotics
645 and grown shaking at 37°C for 14-16 hours. Overnight cultures were back diluted to an OD_{600} of
646 0.06 in fresh LB-Lennox and grown shaking for 2.5 hours, then back diluted to an OD_{600} of 0.06
647 in 5 mL LB-Miller (SPI-1 inducing) or LB-Lennox (control) and grown shaking for 4 hours. One
648 hour prior to infection, HeLa cells were washed three times with imaging media (1x FluoroBrite
649 DMEM, 1% FBS, 2 mM GlutaMAX) to remove residual Penicillin/Streptomycin and 100µl of
650 imaging media was added to each well. Bacterial cultures were pelleted, resuspended in PBS,
651 and diluted to the indicated multiplicity of infection (MOI). 5µl of bacteria was added to each well
652 and the plate was incubated at 37˚C for 30 minutes. HeLa cells were washed three times with

653 imaging media to remove extracellular bacteria, and 200µl of imaging media containing 10 µg/mL
654 gentamicin was added to each well. Plates were sealed with an AeraSeal film and imaged.
655 Imaging was performed with a Nikon Ti2E fluorescence microscope equipped with a Prime BSI
656 sCMOS camera, a SPECTRA III light engine, temperature (37˚C) and environmental (5% CO_2)
657 control. Images were acquired using a 20x/0.95 numerical aperture objective with 2x2 binning.
658 Acquisition was controlled by Nikon Elements software.

659 **Image Analysis**

660 Nuclei labeled with H2B-miRFP670 were segmented using Cellpose3 and a custom trained model
661 [84,85]. Images with sparse nuclei were poorly segmented due to Cellpose's standard image
662 normalization and were manually identified and excluded from analysis. All segmented images
663 were manually inspected, and missegmented nuclei were removed. Bacteria labeled with mRuby2
664 were preprocessed to subtract background and reduce noise using 1) N4 bias field correction
665 algorithm, 2) wavelet-based background subtraction, and 3) anisotropic diffusion [86,87]. Nuclei
666 labels were filtered to remove objects <266 pixels in area (1st percentile of all nuclei). To minimize
667 detection of out-of-focus extracellular bacteria, images were further processed using background
668 subtraction (napari-segment-blobs-and-things-with-membranes: nsbatwm) followed by Laplacian
669 of Gaussian filtering (napari-pyclesperanto-assistant) [88]. Bacteria were segmented using
670 Voronoi-Otsu labeling (pyclesperanto-prototype). A minimum threshold for bacteria object
671 intensity (2500 AU) was determined from uninfected control wells. Bacterial objects were
672 assigned to the nearest nucleus using a Euclidean distance threshold of 60 pixels. Features of
673 nuclei and bacterial objects were extracted using scikit-image regionprops and stored in xarray
674 format. Plots were generated using Seaborn and Matplotlib in Python. Statistical analyses were
675 performed in Python (scipy and statsmodels) using two-way ANOVA with strain and MOI as
676 factors.

677 **Experimental Evolution**

678 Glycerol stocks of WT and T110A strains were streaked on LB agar and incubated overnight at
679 37˚C. Six independent colonies from each strain were inoculated into 3 mL M9/Glc/CAA and
680 grown shaking overnight at 37˚C. The following day, 1 mL of each culture was pelleted (6000rpm,
681 2 minutes) and washed twice in 1 mL MgM-MES to remove residual M9/Glc/CAA. Washed cells
682 were diluted 1:100 (150µl in 15 mL MgM-MES in 125 mL flasks) and grown shaking at 37˚C for
683 approximately 24 hours. For 30 days, 150µl of each culture was transferred daily into 15 mL fresh
684 MgM-MES (1:100) without washing. Glycerol stocks were prepared daily to facilitate subsequent
685 growth assays and whole-genome sequencing.

686 **Statistical Analysis**

687 *Growth curves:* Pairwise comparisons used two-sided, unpaired t-tests and p values were
688 adjusted for multiple comparisons using the Benjamini-Hochberg FDR method. *Flow cytometry:*
689 Comparisons of % GFP(+) cells used a linear mixed-effects model with post-hoc pairwise
690 comparisons performed with unpaired t-tests and Holm-Sidak correction for multiple comparisons.
691 Consistency in trends across replicates was assessed using sign tests. *HeLa cell infection:*
692 Comparisons of infected cell frequency and number of multi-bacteria infection events were
693 performed using two-way ANOVA with strain and MOI as factors. Statistical analyses were
694 performed in Python (scipy and statsmodels). Alpha set to 0.05. All statistical analyses are
695 reported in Table S2.

696

697 **REFERENCES**

698 1. Connolly JPR, Slater SL, O'Boyle N, Goldstone RJ, Crepin VF, Ruano-Gallego D, et al.
699 Host-associated niche metabolism controls enteric infection through fine-tuning the
700 regulation of type 3 secretion. Nat Commun. 2018;9: 4187. doi:10.1038/s41467-018-
701 06701-4
702 2. Fang FC, Frawley ER, Tapscott T, Vázquez-Torres A. Bacterial Stress Responses during
703 Host Infection. Cell Host & Microbe. 2016;20: 133–143. doi:10.1016/j.chom.2016.07.009
704 3. King AN, de Mets F, Brinsmade SR. Who's in control? Regulation of metabolism and
705 pathogenesis in space and time. Current Opinion in Microbiology. 2020;55: 88–96.
706 doi:10.1016/j.mib.2020.05.009
707 4. Laughlin RC, Knodler LA, Barhoumi R, Payne HR, Wu J, Gomez G, et al. Spatial
708 Segregation of Virulence Gene Expression during Acute Enteric Infection with Salmonella
709 enterica serovar Typhimurium. mBio. 2014;5: e00946-13. doi:10.1128/mBio.00946-13
710 5. Sturm A, Heinemann M, Arnoldini M, Benecke A, Ackermann M, Benz M, et al. The Cost of
711 Virulence: Retarded Growth of Salmonella Typhimurium Cells Expressing Type III
712 Secretion System 1. PLOS Pathogens. 2011;7: e1002143.
713 doi:10.1371/journal.ppat.1002143
714 6. Sobota M, Rodilla Ramirez PN, Cambré A, Rocker A, Mortier J, Gervais T, et al. The
715 expression of virulence genes increases membrane permeability and sensitivity to
716 envelope stress in Salmonella Typhimurium. PLoS Biol. 2022;20: e3001608.
717 doi:10.1371/journal.pbio.3001608

718 7. Davis KM. For the Greater (Bacterial) Good: Heterogeneous Expression of Energetically
719 Costly Virulence Factors. Infection and Immunity. 2020;88: e00911-19.
720 doi:10.1128/IAI.00911-19
721 8. Dillon SC, Dorman CJ. Bacterial nucleoid-associated proteins, nucleoid structure and gene
722 expression. Nat Rev Microbiol. 2010;8: 185–195. doi:10.1038/nrmicro2261
723 9. Browning DF, Grainger DC, Busby SJ. Effects of nucleoid-associated proteins on bacterial
724 chromosome structure and gene expression. Current Opinion in Microbiology. 2010;13:
725 773–780. doi:10.1016/j.mib.2010.09.013
726 10. Winardhi RS, Yan J, Kenney LJ. H-NS Regulates Gene Expression and Compacts the
727 Nucleoid: Insights from Single-Molecule Experiments. Biophys J. 2015;109: 1321–1329.
728 doi:10.1016/j.bpj.2015.08.016
729 11. Dorman CJ. H-NS, the genome sentinel. Nat Rev Microbiol. 2007;5: 157–161.
730 doi:10.1038/nrmicro1598
731 12. Arold ST, Leonard PG, Parkinson GN, Ladbury JE. H-NS forms a superhelical protein
732 scaffold for DNA condensation. Proc Natl Acad Sci U S A. 2010;107: 15728–15732.
733 doi:10.1073/pnas.1006966107
734 13. Badaut C, Williams R, Arluison V, Bouffartigues E, Robert B, Buc H, et al. The Degree of
735 Oligomerization of the H-NS Nucleoid Structuring Protein Is Related to Specific Binding to
736 DNA*. Journal of Biological Chemistry. 2002;277: 41657–41666.
737 doi:10.1074/jbc.M206037200
738 14. Owen-Hughes TA, Pavitt GD, Santos DS, Sidebotham JM, Hulton CSJ, Hinton JCD, et al.
739 The chromatin-associated protein H-NS interacts with curved DNA to influence DNA
740 topology and gene expression. Cell. 1992;71: 255–265. doi:10.1016/0092-8674(92)90354-
741 F
742 15. Gordon BRG, Li Y, Cote A, Weirauch MT, Ding P, Hughes TR, et al. Structural basis for
743 recognition of AT-rich DNA by unrelated xenogeneic silencing proteins. Proceedings of the
744 National Academy of Sciences. 2011;108: 10690–10695. doi:10.1073/pnas.1102544108
745 16. Navarre WW, Porwollik S, Wang Y, McClelland M, Rosen H, Libby SJ, et al. Selective
746 Silencing of Foreign DNA with Low GC Content by the H-NS Protein in Salmonella.
747 Science. 2006;313: 236–238. doi:10.1126/science.1128794
748 17. van der Valk RA, Vreede J, Qin L, Moolenaar GF, Hofmann A, Goosen N, et al.
749 Mechanism of environmentally driven conformational changes that modulate H-NS DNA-
750 bridging activity. Storz G, editor. eLife. 2017;6: e27369. doi:10.7554/eLife.27369

751 18. Lucchini S, Rowley G, Goldberg MD, Hurd D, Harrison M, Hinton JCD. H-NS Mediates the
752 Silencing of Laterally Acquired Genes in Bacteria. PLOS Pathogens. 2006;2: e81.
753 doi:10.1371/journal.ppat.0020081
754 19. Porwollik S, Santiviago CA, Cheng P, Long F, Desai P, Fredlund J, et al. Defined Single-
755 Gene and Multi-Gene Deletion Mutant Collections in Salmonella enterica sv Typhimurium.
756 PLOS ONE. 2014;9: e99820. doi:10.1371/journal.pone.0099820
757 20. Wilmes-Riesenberg MR, Foster JW, Curtiss R. An altered rpoS allele contributes to the
758 avirulence of Salmonella typhimurium LT2. Infection and Immunity. 1997;65: 203–210.
759 doi:10.1128/iai.65.1.203-210.1997
760 21. Baba T, Ara T, Hasegawa M, Takai Y, Okumura Y, Baba M, et al. Construction of
761 Escherichia coli K-12 in-frame, single-gene knockout mutants: the Keio collection. Mol Syst
762 Biol. 2006;2: 2006.0008. doi:10.1038/msb4100050
763 22. Dersch P, Kneip S, Bremer E. The nucleoid-associated DNA-binding protein H-NS is
764 required for the efficient adaptation of Escherichia coli K-12 to a cold environment. Molec
765 Gen Genet. 1994;245: 255–259. doi:10.1007/BF00283274
766 23. Walthers D, Li Y, Liu Y, Anand G, Yan J, Kenney LJ. Salmonella enterica Response
767 Regulator SsrB Relieves H-NS Silencing by Displacing H-NS Bound in Polymerization
768 Mode and Directly Activates Transcription *. Journal of Biological Chemistry. 2011;286:
769 1895–1902. doi:10.1074/jbc.M110.164962
770 24. Martínez LC, Banda MM, Fernández-Mora M, Santana FJ, Bustamante VH. HilD Induces
771 Expression of Salmonella Pathogenicity Island 2 Genes by Displacing the Global Negative
772 Regulator H-NS from ssrAB. Journal of Bacteriology. 2014;196: 3746–3755.
773 doi:10.1128/jb.01799-14
774 25. Stoebel DM, Free A, Dorman CJ. Anti-silencing: overcoming H-NS-mediated repression of
775 transcription in Gram-negative enteric bacteria. Microbiology. 2008;154: 2533–2545.
776 doi:10.1099/mic.0.2008/020693-0
777 26. Spratt MR, Lane K. Navigating Environmental Transitions: the Role of Phenotypic Variation
778 in Bacterial Responses. mBio. 2022; e0221222. doi:10.1128/mbio.02212-22
779 27. Ackermann M. A functional perspective on phenotypic heterogeneity in microorganisms.
780 Nat Rev Microbiol. 2015;13: 497–508. doi:10.1038/nrmicro3491
781 28. Weigel WA, Dersch P. Phenotypic heterogeneity: a bacterial virulence strategy. Microbes
782 and Infection. 2018;20: 570–577. doi:10.1016/j.micinf.2018.01.008
783 29. Hansen-Wester I, Hensel M. Salmonella pathogenicity islands encoding type III secretion
784 systems. Microbes and Infection. 2001;3: 549–559. doi:10.1016/S1286-4579(01)01411-3

785 30. Arnoldini M, Vizcarra IA, Peña-Miller R, Stocker N, Diard M, Vogel V, et al. Bistable
786 Expression of Virulence Genes in Salmonella Leads to the Formation of an Antibiotic-
787 Tolerant Subpopulation. Balaban N, editor. PLoS Biol. 2014;12: e1001928.
788 doi:10.1371/journal.pbio.1001928
789 31. Hautefort I, Proença MJ, Hinton JCD. Single-Copy Green Fluorescent Protein Gene
790 Fusions Allow Accurate Measurement of Salmonella Gene Expression In Vitro and during
791 Infection of Mammalian Cells. Applied and Environmental Microbiology. 2003;69: 7480–
792 7491. doi:10.1128/AEM.69.12.7480-7491.2003
793 32. Diard M, Garcia V, Maier L, Remus-Emsermann MNP, Regoes RR, Ackermann M, et al.
794 Stabilization of cooperative virulence by the expression of an avirulent phenotype. Nature.
795 2013;494: 353–356. doi:10.1038/nature11913
796 33. Spratt M, Lane K. Temporal tuning of switch-like virulence expression resolves
797 environmental uncertainty through phenotypic heterogeneity. bioRxiv. 2025;
798 2025.07.01.662634. doi:10.1101/2025.07.01.662634
799 34. Fields PI, Swanson RV, Haidaris CG, Heffron F. Mutants of Salmonella typhimurium that
800 cannot survive within the macrophage are avirulent. Proc Natl Acad Sci U S A. 1986;83:
801 5189–5193. doi:10.1073/pnas.83.14.5189
802 35. Cirillo DM, Valdivia RH, Monack DM, Falkow S. Macrophage-dependent induction of the
803 Salmonella pathogenicity island 2 type III secretion system and its role in intracellular
804 survival. Molecular Microbiology. 1998;30: 175–188. doi:10.1046/j.1365-
805 2958.1998.01048.x
806 36. Han J, Aljahdali N, Zhao S, Tang H, Harbottle H, Hoffmann M, et al. Infection biology of
807 Salmonella enterica. EcoSal Plus. 2024;12: eesp-0001-2023. doi:10.1128/ecosalplus.esp-
808 0001-2023
809 37. Blair JMA, Richmond GE, Bailey AM, Ivens A, Piddock LJV. Choice of Bacterial Growth
810 Medium Alters the Transcriptome and Phenotype of Salmonella enterica Serovar
811 Typhimurium. Roe AJ, editor. PLoS ONE. 2013;8: e63912.
812 doi:10.1371/journal.pone.0063912
813 38. Reuter T, Scharte F, Franzkoch R, Liss V, Hensel M. Single cell analyses reveal distinct
814 adaptation of typhoidal and non-typhoidal Salmonella enterica serovars to intracellular
815 lifestyle. PLOS Pathogens. 2021;17: e1009319. doi:10.1371/journal.ppat.1009319
816 39. Stapels DAC, Hill PWS, Westermann AJ, Fisher RA, Thurston TL, Saliba A-E, et al.
817 Salmonella persisters undermine host immune defenses during antibiotic treatment.
818 Science. 2018;362: 1156–1160. doi:10.1126/science.aat7148

40. Ali SS, Soo J, Rao C, Leung AS, Ngai DH-M, Ensminger AW, et al. Silencing by H-NS Potentiated the Evolution of Salmonella. PLOS Pathogens. 2014;10: e1004500. doi:10.1371/journal.ppat.1004500
41. Higashi K, Tobe T, Kanai A, Uyar E, Ishikawa S, Suzuki Y, et al. H-NS Facilitates Sequence Diversification of Horizontally Transferred DNAs during Their Integration in Host Chromosomes. PLOS Genetics. 2016;12: e1005796. doi:10.1371/journal.pgen.1005796
42. Dorman CJ. H-NS: a universal regulator for a dynamic genome. Nature Reviews Microbiology. 2004;2: 391–400. doi:10.1038/nrmicro883
43. Dorman CJ, Hinton JCD, Free A. Domain organization and oligomerization among H-NS-like nucleoid-associated proteins in bacteria. Trends in Microbiology. 1999;7: 124–128. doi:10.1016/S0966-842X(99)01455-9
44. Riccardi E, van Mastbergen EC, Navarre WW, Vreede J. Predicting the mechanism and rate of H-NS binding to AT-rich DNA. PLoS Comput Biol. 2019;15: e1006845. doi:10.1371/journal.pcbi.1006845
45. Li S, Liu Q, Duan C, Li J, Sun H, Xu L, et al. c-di-GMP inhibits the DNA binding activity of H-NS in Salmonella. Nat Commun. 2023;14: 7502. doi:10.1038/s41467-023-43442-5
46. Ali SS, Whitney JC, Stevenson J, Robinson H, Howell PL, Navarre WW. Structural Insights into the Regulation of Foreign Genes in *Salmonella* by the Hha/H-NS Complex*. Journal of Biological Chemistry. 2013;288: 13356–13369. doi:10.1074/jbc.M113.455378
47. Ueguchi C, Suzuki T, Yoshida T, Tanaka K, Mizuno T. Systematic Mutational Analysis Revealing the Functional Domain Organization ofEscherichia coliNucleoid Protein H-NS. Journal of Molecular Biology. 1996;263: 149–162. doi:10.1006/jmbi.1996.0566
48. Donato GM, Kawula TH. Phenotypic Analysis of Random hns Mutations Differentiate DNA-Binding Activity from Properties of fimA Promoter Inversion Modulation and Bacterial Motility. J Bacteriol. 1999;181: 941–948. doi:10.1128/jb.181.3.941-948.1999
49. Smits WK, Kuipers OP, Veening J-W. Phenotypic variation in bacteria: the role of feedback regulation. Nat Rev Microbiol. 2006;4: 259–271. doi:10.1038/nrmicro1381
50. To T-L, Maheshri N. Noise Can Induce Bimodality in Positive Transcriptional Feedback Loops Without Bistability. Science. 2010;327: 1142–1145. doi:10.1126/science.1178962
51. Chalancon G, Ravarani CNJ, Balaji S, Martinez-Arias A, Aravind L, Jothi R, et al. Interplay between gene expression noise and regulatory network architecture. Trends in Genetics. 2012;28: 221–232. doi:10.1016/j.tig.2012.01.006
52. Eldar A, Elowitz MB. Functional roles for noise in genetic circuits. Nature. 2010;467: 167–173. doi:10.1038/nature09326

853 53. Ibarra JA, Knodler LA, Sturdevant DE, Virtaneva K, Carmody AB, Fischer ER, et al.
854 Induction of Salmonella pathogenicity island 1 under different growth conditions can affect
855 Salmonella–host cell interactions in vitro. Microbiology. 2010;156: 1120–1133.
856 doi:10.1099/mic.0.032896-0
857 54. Collazo CM, Galán JE. Requirement for exported proteins in secretion through the
858 invasion-associated type III system of Salmonella typhimurium. Infection and Immunity.
859 1996;64: 3524–3531. doi:10.1128/iai.64.9.3524-3531.1996
860 55. Galán JE, Curtiss R. Cloning and molecular characterization of genes whose products
861 allow Salmonella typhimurium to penetrate tissue culture cells. Proceedings of the National
862 Academy of Sciences. 1989;86: 6383–6387. doi:10.1073/pnas.86.16.6383
863 56. Lou L, Zhang P, Piao R, Wang Y. Salmonella Pathogenicity Island 1 (SPI-1) and Its
864 Complex Regulatory Network. Front Cell Infect Microbiol. 2019;9.
865 doi:10.3389/fcimb.2019.00270
866 57. Kim JM, Garcia-Alcala M, Balleza E, Cluzel P. Stochastic transcriptional pulses orchestrate
867 flagellar biosynthesis in *Escherichia coli*. Sci Adv. 2020;6: eaax0947.
868 doi:10.1126/sciadv.aax0947
869 58. Sánchez-Romero MA, Casadesús J. Contribution of SPI-1 bistability to Salmonella
870 enterica cooperative virulence: insights from single cell analysis. Sci Rep. 2018;8: 14875.
871 doi:10.1038/s41598-018-33137-z
872 59. Misselwitz B, Barrett N, Kreibich S, Vonaesch P, Andritschke D, Rout S, et al. Near
873 Surface Swimming of Salmonella Typhimurium Explains Target-Site Selection and
874 Cooperative Invasion. PLOS Pathogens. 2012;8: e1002810.
875 doi:10.1371/journal.ppat.1002810
876 60. Garmendia J, Beuzón CR, Ruiz-Albert J, Holden DW. The roles of SsrA–SsrB and OmpR–
877 EnvZ in the regulation of genes encoding the Salmonella typhimurium SPI-2 type III
878 secretion system. Microbiology. 2003;149: 2385–2396. doi:10.1099/mic.0.26397-0
879 61. Bijlsma JJE, Groisman EA. The PhoP/PhoQ system controls the intramacrophage type
880 three secretion system of *Salmonella enterica*. Molecular Microbiology. 2005;57: 85–96.
881 doi:10.1111/j.1365-2958.2005.04668.x
882 62. Fass E, Groisman EA. Control of Salmonella pathogenicity island-2 gene expression.
883 Current Opinion in Microbiology. 2009;12: 199–204. doi:10.1016/j.mib.2009.01.004
884 63. Nickerson CA, Curtiss R. Role of sigma factor RpoS in initial stages of Salmonella
885 typhimurium infection. Infect Immun. 1997;65: 1814–1823. doi:10.1128/iai.65.5.1814-
886 1823.1997

887 64. Soo Lee I, Lin J, Hall HK, Bearson B, Foster JW. The stationary-phase sigma factor σS
888 (RpoS) is required for a sustained acid tolerance response in virulent Salmonella
889 typhimurium. Molecular Microbiology. 1995;17: 155–167. doi:10.1111/j.1365-
890 2958.1995.mmi_17010155.x
891 65. Battesti A, Tsegaye YM, Packer DG, Majdalani N, Gottesman S. H-NS Regulation of IraD
892 and IraM Antiadaptors for Control of RpoS Degradation. Journal of Bacteriology. 2012;194:
893 2470–2478. doi:10.1128/jb.00132-12
894 66. Pang PP, Lundberg AS, Walker GC. Identification and characterization of the mutL and
895 mutS gene products of Salmonella typhimurium LT2. Journal of Bacteriology. 1985;163:
896 1007–1015. doi:10.1128/jb.163.3.1007-1015.1985
897 67. Westermann AJ, Venturini E, Sellin ME, Förstner KU, Hardt W-D, Vogel J. The Major RNA-
898 Binding Protein ProQ Impacts Virulence Gene Expression in Salmonella enterica Serovar
899 Typhimurium. mBio. 2019;10: e02504-18. doi:10.1128/mBio.02504-18
900 68. Bergman S, Andresen L, Kjellin J, Martinez Burgo Y, Geiser P, Baars S, et al. ProQ-
901 dependent activation of Salmonella virulence genes mediated by post-transcriptional
902 control of PhoP synthesis. mSphere. 2024;9: e00018-24. doi:10.1128/msphere.00018-24
903 69. Gal-Mor O, Finlay BB. Pathogenicity islands: a molecular toolbox for bacterial virulence.
904 Cellular Microbiology. 2006;8: 1707–1719. doi:10.1111/j.1462-5822.2006.00794.x
905 70. Pennings PS, Ogbunugafor CB, Hershberg R. Reversion is most likely under high mutation
906 supply when compensatory mutations do not fully restore fitness costs. G3 (Bethesda).
907 2022;12: jkac190. doi:10.1093/g3journal/jkac190
908 71. Yu X-J, Liu M, Holden DW. SsaM and SpiC interact and regulate secretion of Salmonella
909 Pathogenicity Island 2 type III secretion system effectors and translocators. Molecular
910 Microbiology. 2004;54: 604–619. doi:10.1111/j.1365-2958.2004.04297.x
911 72. Beuzón CR, Banks G, Deiwick J, Hensel M, Holden DW. pH-dependent secretion of SseB,
912 a product of the SPI-2 type III secretion system of Salmonella typhimurium. Molecular
913 Microbiology. 1999;33: 806–816. doi:10.1046/j.1365-2958.1999.01527.x
914 73. Moore SJ, Lai H-E, Kelwick RJR, Chee SM, Bell DJ, Polizzi KM, et al. EcoFlex: A
915 Multifunctional MoClo Kit for *E. coli* Synthetic Biology. ACS Synth Biol. 2016;5: 1059–1069.
916 doi:10.1021/acssynbio.6b00031
917 74. Warren DJ. Preparation of highly efficient electrocompetent *Escherichia coli* using
918 glycerol/mannitol density step centrifugation. Analytical Biochemistry. 2011;413: 206–207.
919 doi:10.1016/j.ab.2011.02.036

75. Montaño-Gutierrez LF, Moreno NM, Farquhar IL, Huo Y, Bandiera L, Swain PS. Analysing and meta-analysing time-series data of microbial growth and gene expression from plate readers. Marz M, editor. PLoS Comput Biol. 2022;18: e1010138. doi:10.1371/journal.pcbi.1010138
76. Waskom ML. seaborn: statistical data visualization. Journal of Open Source Software. 2021;6: 3021. doi:10.21105/joss.03021
77. Hunter JD. Matplotlib: A 2D Graphics Environment. Computing in Science & Engineering. 2007;9: 90–95. doi:10.1109/MCSE.2007.55
78. Deatherage DE, Barrick JE. Identification of mutations in laboratory evolved microbes from next-generation sequencing data using breseq. Methods Mol Biol. 2014;1151: 165–188. doi:10.1007/978-1-4939-0554-6_12
79. Tendeng C, Badaut C, Krin E, Gounon P, Ngo S, Danchin A, et al. Isolation and Characterization of vicH, Encoding a New Pleiotropic Regulator in Vibrio cholerae. Journal of Bacteriology. 2000;182: 2026–2032. doi:10.1128/jb.182.7.2026-2032.2000
80. Sievers F, Wilm A, Dineen D, Gibson TJ, Karplus K, Li W, et al. Fast, scalable generation of high-quality protein multiple sequence alignments using Clustal Omega. Mol Syst Biol. 2011;7: 539. doi:10.1038/msb.2011.75
81. Waterhouse AM, Procter JB, Martin DMA, Clamp M, Barton GJ. Jalview Version 2—a multiple sequence alignment editor and analysis workbench. Bioinformatics. 2009;25: 1189–1191. doi:10.1093/bioinformatics/btp033
82. Meng EC, Goddard TD, Pettersen EF, Couch GS, Pearson ZJ, Morris JH, et al. UCSF ChimeraX: Tools for structure building and analysis. Protein Science. 2023;32: e4792. doi:10.1002/pro.4792
83. Schindelin J, Arganda-Carreras I, Frise E, Kaynig V, Longair M, Pietzsch T, et al. Fiji: an open-source platform for biological-image analysis. Nat Methods. 2012;9: 676–682. doi:10.1038/nmeth.2019
84. Stringer C, Wang T, Michaelos M, Pachitariu M. Cellpose: a generalist algorithm for cellular segmentation. Nat Methods. 2021;18: 100–106. doi:10.1038/s41592-020-01018-x
85. Pachitariu M, Stringer C. Cellpose 2.0: how to train your own model. Nat Methods. 2022;19: 1634–1641. doi:10.1038/s41592-022-01663-4
86. Kudo T, Jeknić S, Macklin DN, Akhter S, Hughey JJ, Regot S, et al. Live-cell measurements of kinase activity in single cells using translocation reporters. Nat Protoc. 2018;13: 155–169. doi:10.1038/nprot.2017.128

87. Galloway CM, Ru ECL, Etchegoin PG. An Iterative Algorithm for Background Removal in Spectroscopy by Wavelet Transforms. Appl Spectrosc. 2009;63: 1370–1376. doi:10.1366/000370209790108905
88. Rigaud S, Haase R, Soltwedel J, grahamross123, Albert M, Rajasekhar P. clEsperanto/pyclesperanto: 0.16.0. Zenodo; 2024. doi:10.5281/zenodo.14199059

Figure 1. Identification of an H-NS DNA-binding domain mutation in a *Salmonella* strain with impaired growth in SPI-2-inducing conditions (A) (i) The mutant strain exhibits growth defects in SPI-2-inducing conditions. Wildtype (WT, gray) and mutant (MUT, magenta) strains were grown in non-SPI-2-inducing media (M9/Glc/CAA) or SPI-2-inducing media (MgM-MES), and OD_{600} was recorded using a plate reader. Growth curves show averages of three independent experiments, each with three technical replicates; shaded regions represent standard deviation. Media control is shown in black. Y-axes are scaled to the growth condition. (ii) Growth metrics extracted from data in (i). Individual datapoints represent independent experiments. Asterisks denote significance as determined by two-sided unpaired t-test with Benjamini-Hochberg FDR correction as follows: ** $p<0.01$; ns, not significant. (B) The MUT strain contains a mutation in the conserved DNA-binding domain (DBD) of H-NS. (i) Schematic showing the genomic location of *hns* in STm and domain organization of the H-NS protein. Arrow indicates the location of the mutation identified by whole genome sequencing. (ii) Multiple sequence alignment showing conservation of the mutated residue (T110, white) across enteric bacteria. Dark blue and asterisks indicate complete conservation.

Figure S1. Growth metrics and whole genome sequencing of the mutant strain (A) Growth curve analysis in additional media conditions. Plate reader growth curves of WT (gray) and MUT (magenta) strains in (i) non-SPI-1-inducing (LB) and SPI-1-inducing (LB-High Salt [LB-HS]) media, and (ii) replete media (M9/Glc/CAA) and nutrient-limited media (M9/Glc). Growth curves show averages of three independent experiments, each with three technical replicates; shaded regions represent standard deviation. Media control is shown in black. Y-axes are scaled to the growth condition. (iii) Growth metrics extracted from the data in (i) and (ii). Individual datapoints represent independent experiments. Asterisks denote significance as determined by two-sided unpaired t-test with Benjamini-Hochberg FDR correction as follows: * $p<0.05$, ** $p<0.01$; ns, not significant. (B) Whole genome sequencing identified *hns* a328g (T110A) as the only coding region difference between the WT and MUT strains.

Figure 1

A (i)

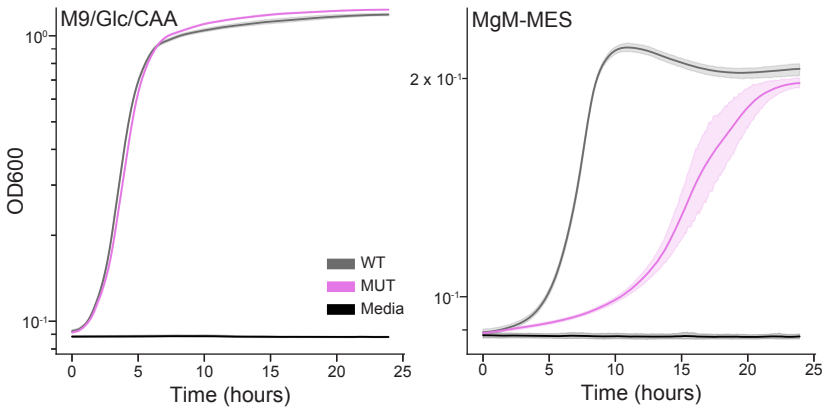

(ii)

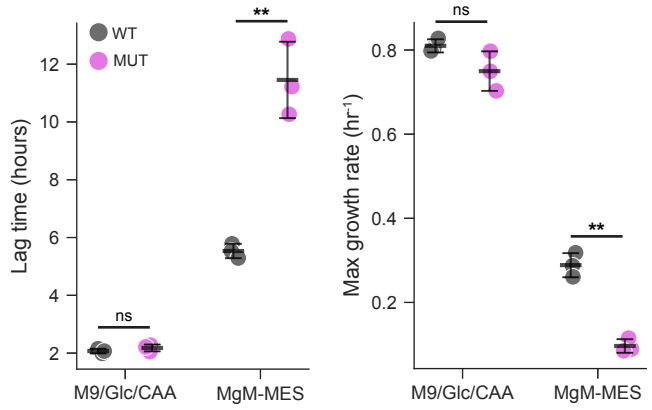

B (i)

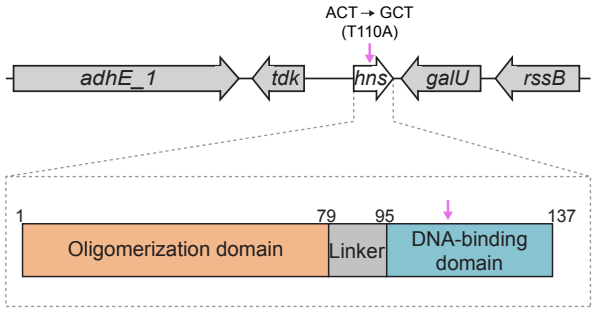

(ii)

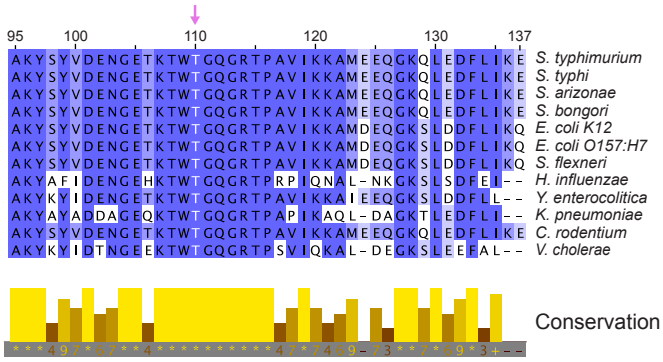

Figure S1

A (i)

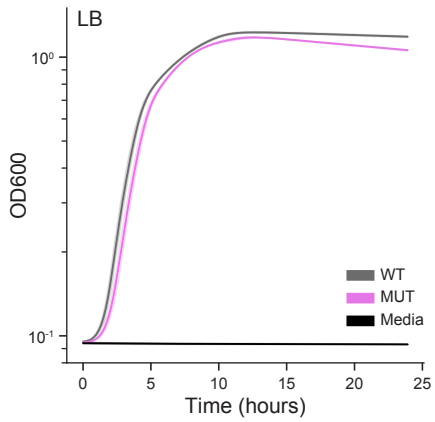

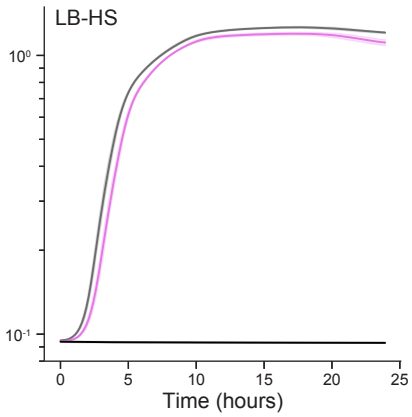

(iii)

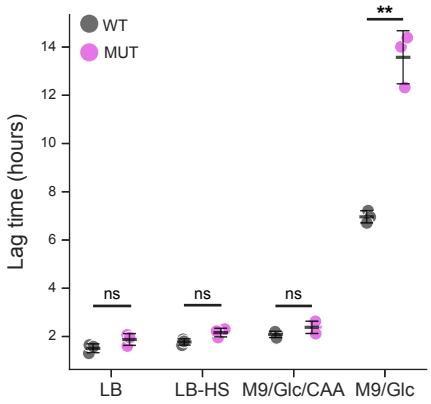

(ii)

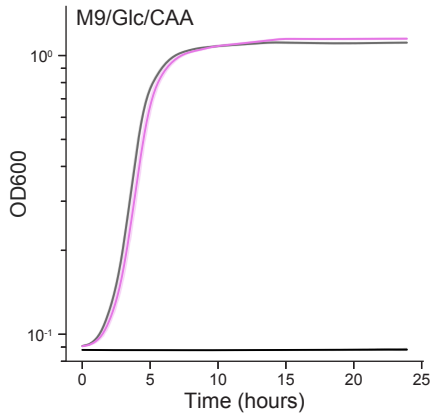

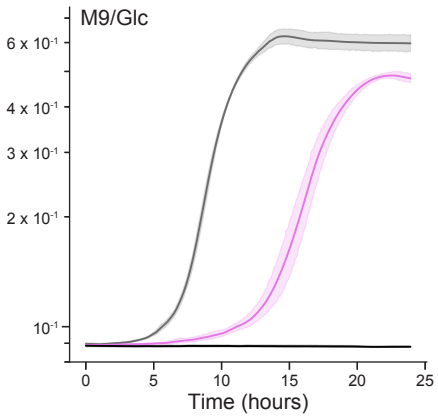

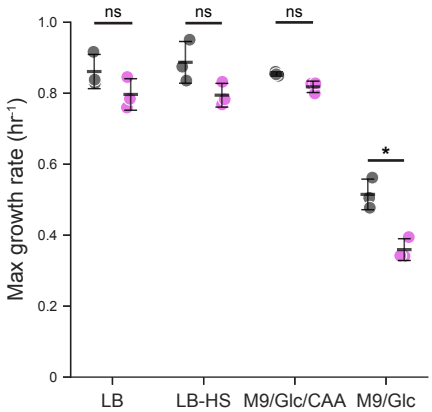

B

Mutant strain WGS results

Position	Mutation	Annotation	Gene	Description
1800432	A → C	intergenic (-53/+59)	STM14_2047 ← / ← STM14_2048	hypothetical protein/hypothetical protein
1858299	A → G	T110A (ACT→GCT)	*hns* →	global DNA-binding transcriptional dual regulator H-NS
3213731	C → A	intergenic (-12/+564)	STM14_3662 ← / ← STM14_3663	conserved hypothetical protein/plasmid maintenance protein
1312881-1312887	new junction	pseudogene (128/365 nt)	STM14_1462	pseudogene (DNA packaging-like protein)

Figure 2. H-NS T110A has reduced DNA-binding affinity compared to H-NS WT (A) Structure of STm H-NS WT and T110A DNA-binding domains modeled in ChimeraX using the NMR structure (PDB: 2L93). The T110A mutation is predicted to disrupt a polar contact (black dashed line) between the Thr110 side chain oxygen and the Gln112 backbone nitrogen. Gln112 is part of the QGR motif (shown in blue), an AT-hook that mediates direct DNA contacts. The mutation is also predicted to disrupt van der Waals interactions (green dashed line) between Thr110 and Trp109, while introducing a new interaction between Ala110 and Lys96. These structural changes may alter the positioning of the QGR motif and reduce its ability to bind the DNA minor groove. (B) Purified H-NS WT and T110A proteins analyzed by SDS-PAGE. Protein was visualized using Coomassie staining. (C) EMSAs demonstrate reduced DNA-binding affinity of H-NS T110A. (i) H-NS WT and T110A proteins were incubated with *ssrAB* promoter DNA at the indicated concentrations for 30 minutes and separated on a 5% native TBE gel. DNA was visualized using SYBR Safe staining. Representative gels are shown for WT (top) and T110A (bottom). (ii) Quantification of EMSA data from panel (i) showing the fraction of DNA-bound H-NS as a function of protein concentration. WT (gray) and T110A (magenta) data points are shown as circles and represent measurements from a single replicate. Lines represent fits to the Hill equation. K_D values shown are means ± standard deviation from four independent experiments.

Figure S2. Biochemical characterization of H-NS T110A (A) Schematic of the plasmid construct used for H-NS protein expression. (B) Full SDS-PAGE gel image corresponding to Figure 2B. (C) Sequence and features of the *ssrAB* promoter region used in EMSAs. Underlined sequences indicate PCR primers used to amplify the region from STm genomic DNA. Colored text highlights AT-rich tracts of potential H-NS binding sites (red: longer tracts, blue: shorter tracts). (D) Complete gel images from four independent EMSA experiments for H-NS WT and T110A proteins. Data from replicate 4 is shown in Figure 2C. (E) Quantification and curve fitting of EMSA data from panel D. Blue circles represent experimental data. Lines represent fits to the Hill equation. K_D values are reported as best fit ± SE (standard error).

Figure 2

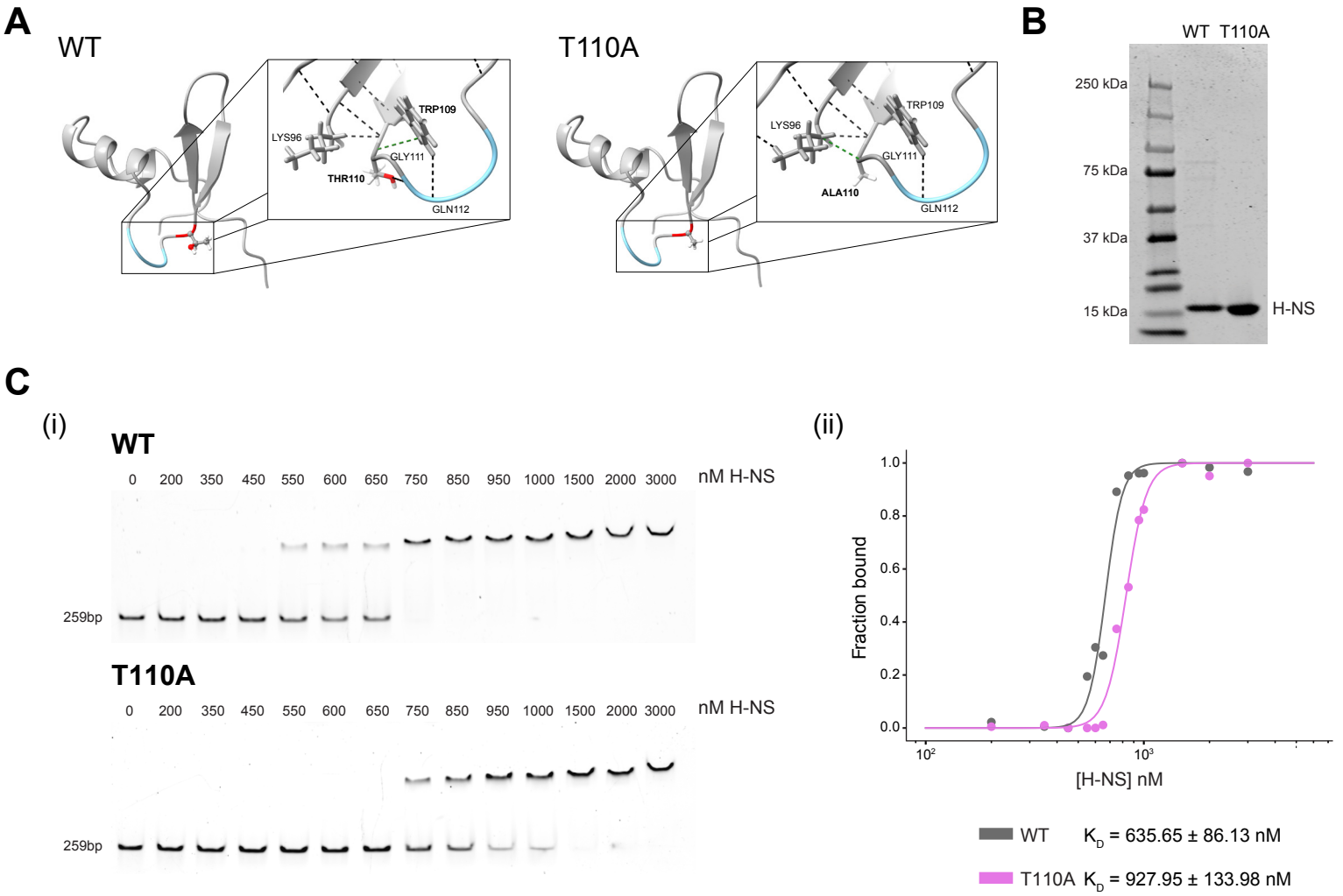
A
WT
LYS96
TRP109
GLY111
THR110
GLN112
T110A
LYS96
TRP109
GLY111
ALA110
GLN112
B
WT T110A
250 kDa
75 kDa
37 kDa
15 kDa
H-NS
C
(i)
WT
0 200 350 450 550 600 650 750 850 950 1000 1500 2000 3000
nM H-NS
259bp
T110A
0 200 350 450 550 600 650 750 850 950 1000 1500 2000 3000
nM H-NS
259bp
(ii)
Fraction bound
1.0
0.8
0.6
0.4
0.2
0.0
10^2
10^3
[H-NS] nM
WT K_D = 635.65 ± 86.13 nM
T110A K_D = 927.95 ± 133.98 nM

Figure S2

A

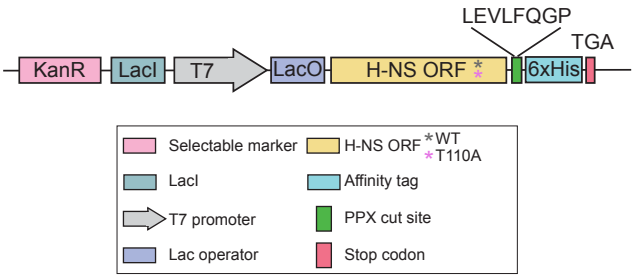

B

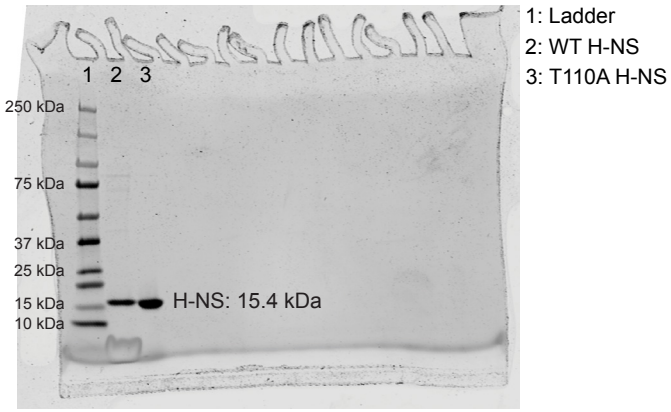

C

P_{ssrAB}: 239-bp, AT content 71.13%

TACAATATCAGGATGCTGTCTACATATACCTTGTCACAGGCGATTCTATCATTCGGATTT
TCCGATAAATTCACAATTACATTTTCAGCATTGACATAAAAACTTACAATTTGAAAAATT
ATTTATTAAATAAACTGTTACGATGTTTTTACATCGCCATCTTATTAAAAAGTAATTGTA
GTCATCGACTGGGTTATATATGAAGAAATTTATCTTCCTAATGATAACACCATCGATTA

Underlined = primer sequence
Red = AT tracts longer than 5bp
Blue = AT tracts that are 5bp

D

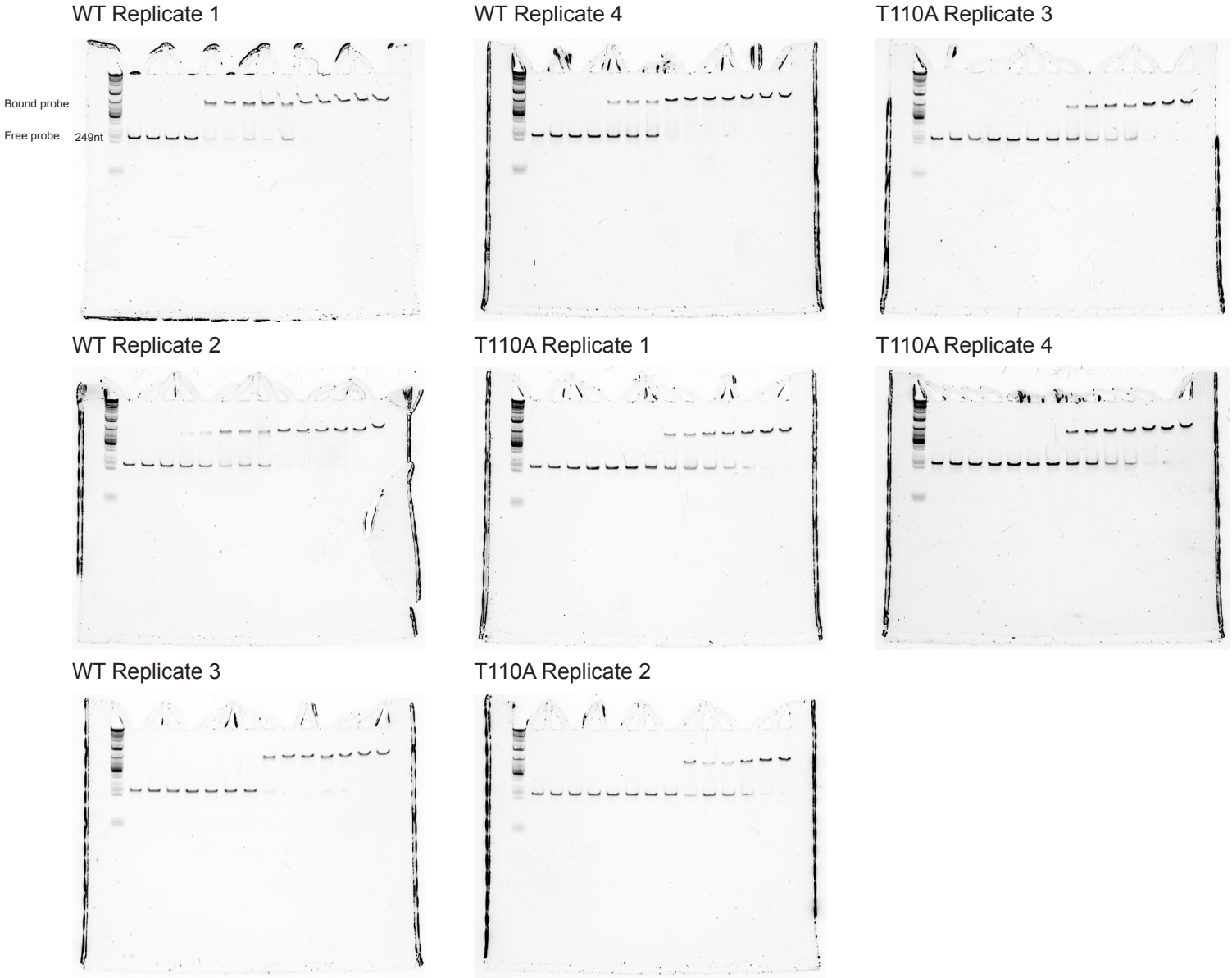

Figure S2

E

(i) **WT**

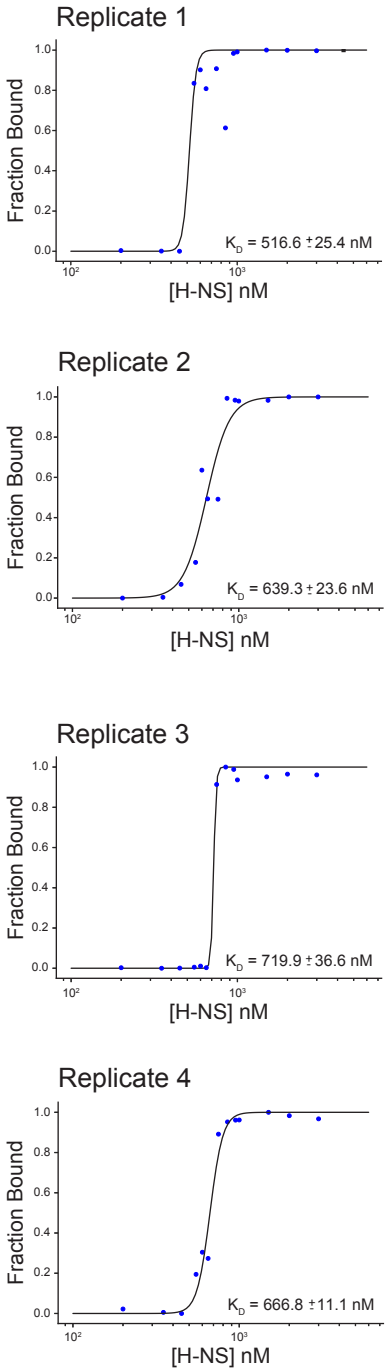

(ii) **T110A**

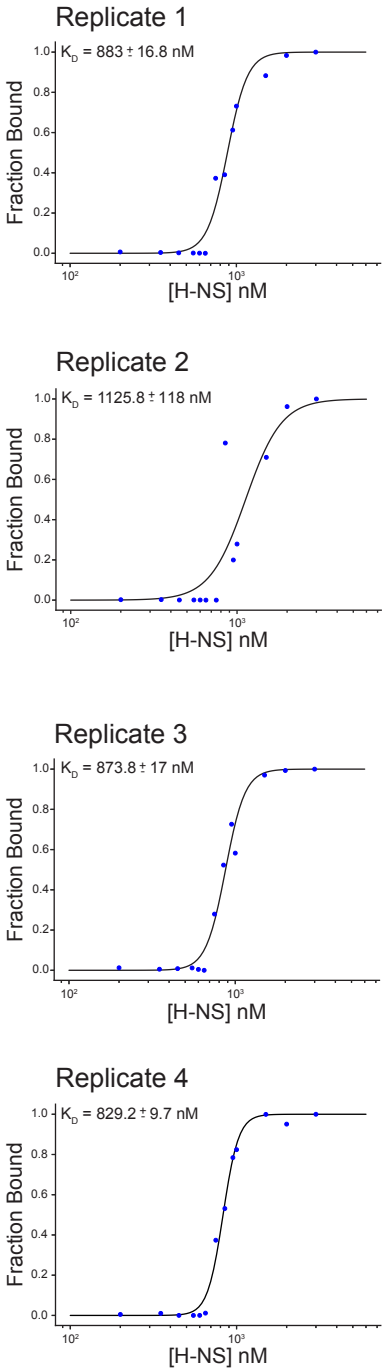

Figure 3. H-NS T110A increases the fraction of virulence-gene expressing cells with functional consequences for infection (A) Schematic illustrating three potential outcomes of reduced H-NS DNA-binding affinity on virulence gene expression heterogeneity. (B) H-NS T110A cells activate the SPI-2 reporter more rapidly and with increased frequency, while maintaining bimodal expression. WT and T110A strains containing the SPI-2 reporter plasmid (P_{ssaG}-sfGFP(LVA)) were grown in SPI-2-inducing media (MgM-MES) and analyzed by flow cytometry. (i) Representative histograms at 4 hours of WT (gray) and T110A (magenta) strains grown in MgM-MES with glycerol (solid line) or glucose (dashed line). GFP(-) control strain is shown in black. (ii) Quantification shows the percentage of GFP(+) cells at 2 and 4 hours. Bars represent the mean ± SD of 5 independent experiments. Individual datapoints are shown in shades of gray. n=50,000 cells per sample. (C) H-NS T110A increases the frequency of SPI-1 responders while maintaining bimodal expression. WT and T110A strains containing the SPI-1 reporter plasmid (P_{invF}-sfGFP) were grown in SPI-1-inducing media (LB High Salt) and non-inducing media (LB) and analyzed by flow cytometry. (i) Representative histograms at 4 hours of WT (gray) and T110A (magenta) strains grown in LB High Salt. GFP(-) control strain is shown in black. (ii) Quantification shows the percentage of GFP(+) cells at 3, 4, and 5 hours. Bars represent the mean ± SD of 3 independent experiments. Individual datapoints are shown in shades of gray. n=50,000 cells per sample. For (B) and (C) asterisks denote significance as determined by linear mixed-effects model with post-hoc pairwise comparisons using unpaired t-tests with Holm-Sidak correction for multiple comparisons: * $p<0.05$, *** $p<0.001$; ns, not significant. (D) (i) Schematic illustrating features of virulence heterogeneity altered in the H-NS T110A strain. (ii) Activation threshold model for how H-NS alters the fraction of cells expressing virulence genes. In the T110A strain, the virulence activation threshold (dotted line) is lowered (pink arrow), increasing the responder fraction (green) while preserving bimodality. (E) H-NS T110A strain enhances epithelial cell infection. H-NS WT and T110A strains expressing constitutive mRuby2 (P_{SJM901}-mRuby2) were used to infect HeLa cells at varying multiplicity of infection (MOI), and infections were imaged and quantified as described in the Methods. (i) Percentage of infected cells. Line represents the mean and circles the individual datapoints from 3 independent experiments. T110A results in an increased frequency of infected cells compared to WT (two-way ANOVA, effect of strain: $F(1,16)=25.1$, $p<0.001$; n=total cells across 3 independent experiments). (ii) Percentage of infected cells that contain multiple bacteria. Line represents the mean and circles the individual datapoints from 3 independent experiments. T110A shows an increased frequency of multi-bacteria infection events (two-way ANOVA, effect of strain: $F(1,8)=6.4$, $p<0.05$; n=total infected cells across 3 independent experiments). Scatter plot shows total intensity versus area of bacterial

masks for infected cells containing multiple bacteria. Individual infected cells are represented as circles, and replicates are shown in shades of gray.

Figure S3. SPI-2 and SPI-1 reporter expression in H-NS T110A strain (A) SPI-2 reporter (P_{ssaG}-sfGFP(LVA)) expression vs growth. Scatter plot shows % GFP(+) cells versus OD_{600} for WT and T110A samples at 4 hours (corresponding to data in Figure 3B) in MgM-MES with glycerol (circles) or glucose (squares) as the carbon source. (B) Mean fluorescence intensity (MFI) of GFP(-) and GFP(+) subpopulations for SPI-2 reporter data shown in Figure 3B. (C) SPI-2 reporter expression under non-inducing conditions. Flow cytometry data was analyzed as in Figure 3B. n=50,000 cells/sample, 5 independent experiments. (D) MFI of GFP(-) and GFP(+) subpopulations for SPI-1 reporter data shown in Figure 3C. (E) SPI-1 reporter (P_{invF}-sfGFP) expression in the T110A strain in non-inducing media. (i) Representative histogram of WT and T110A strains containing the SPI-1 reporter plasmid grown in LB for 4 hours. n=50,000 cells. Data corresponds to Figure 3C. (ii) The frequency of SPI-1 reporter GFP(+) cells before induction was assessed by measuring % GFP(+) cells after the first (BD1) and second (BD2) back dilution in LB and comparing to samples grown in SPI-1-inducing media (LB High Salt) for 3, 4, and 5 hours. SPI-1 reporter expression is negligible before induction in LB High Salt. WT strain shown as gray and T110A as magenta across all panels.

Figure 3

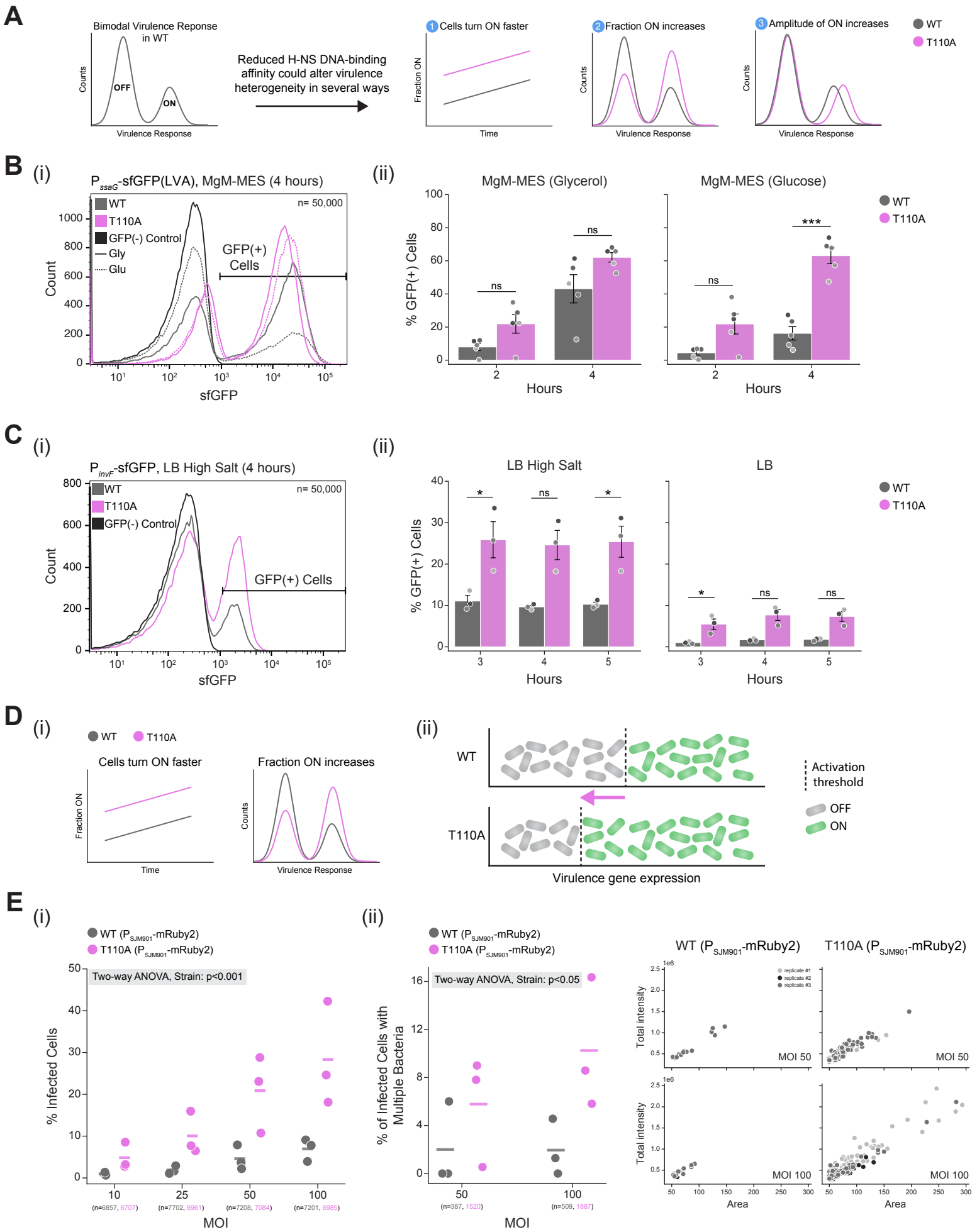
A
Bimodal Virulence Reponse in WT
Counts
OFF
ON
Virulence Response
Reduced H-NS DNA-binding affinity could alter virulence heterogeneity in several ways
1 Cells turn ON faster
Fraction ON
Time
2 Fraction ON increases
Counts
Virulence Response
3 Amplitude of ON increases
Counts
Virulence Response
WT
T110A
B
(i)
P ssaG-sfGFP(LVA), MgM-MES (4 hours)
WT
T110A
GFP(-) Control
Gly
Glu
n= 50,000
GFP(+) Cells
Count
sfGFP
(ii)
MgM-MES (Glycerol)
MgM-MES (Glucose)
% GFP(+) Cells
ns
***
Hours
WT
T110A
C
(i)
P invF-sfGFP, LB High Salt (4 hours)
WT
T110A
GFP(-) Control
n= 50,000
GFP(+) Cells
Count
sfGFP
(ii)
LB High Salt
LB
% GFP(+) Cells
*
ns
Hours
WT
T110A
D
(i)
WT
T110A
Cells turn ON faster
Fraction ON
Time
Fraction ON increases
Counts
Virulence Response
(ii)
WT
T110A
Activation threshold
OFF
ON
Virulence gene expression
E
(i)
WT (P SJM901-mRuby2)
T110A (P SJM901-mRuby2)
Two-way ANOVA, Strain: p<0.001
% Infected Cells
MOI
(n=6857, 6707)
(n=7702, 6961)
(n=7208, 7084)
(n=7201, 6985)
(ii)
WT (P SJM901-mRuby2)
T110A (P SJM901-mRuby2)
Two-way ANOVA, Strain: p<0.05
% of Infected Cells with Multiple Bacteria
MOI
(n=387, 1520)
(n=509, 1887)
WT (P SJM901-mRuby2)
T110A (P SJM901-mRuby2)
replicate #1
replicate #2
replicate #3
Total intensity
MOI 50
MOI 100
Area

Figure S3

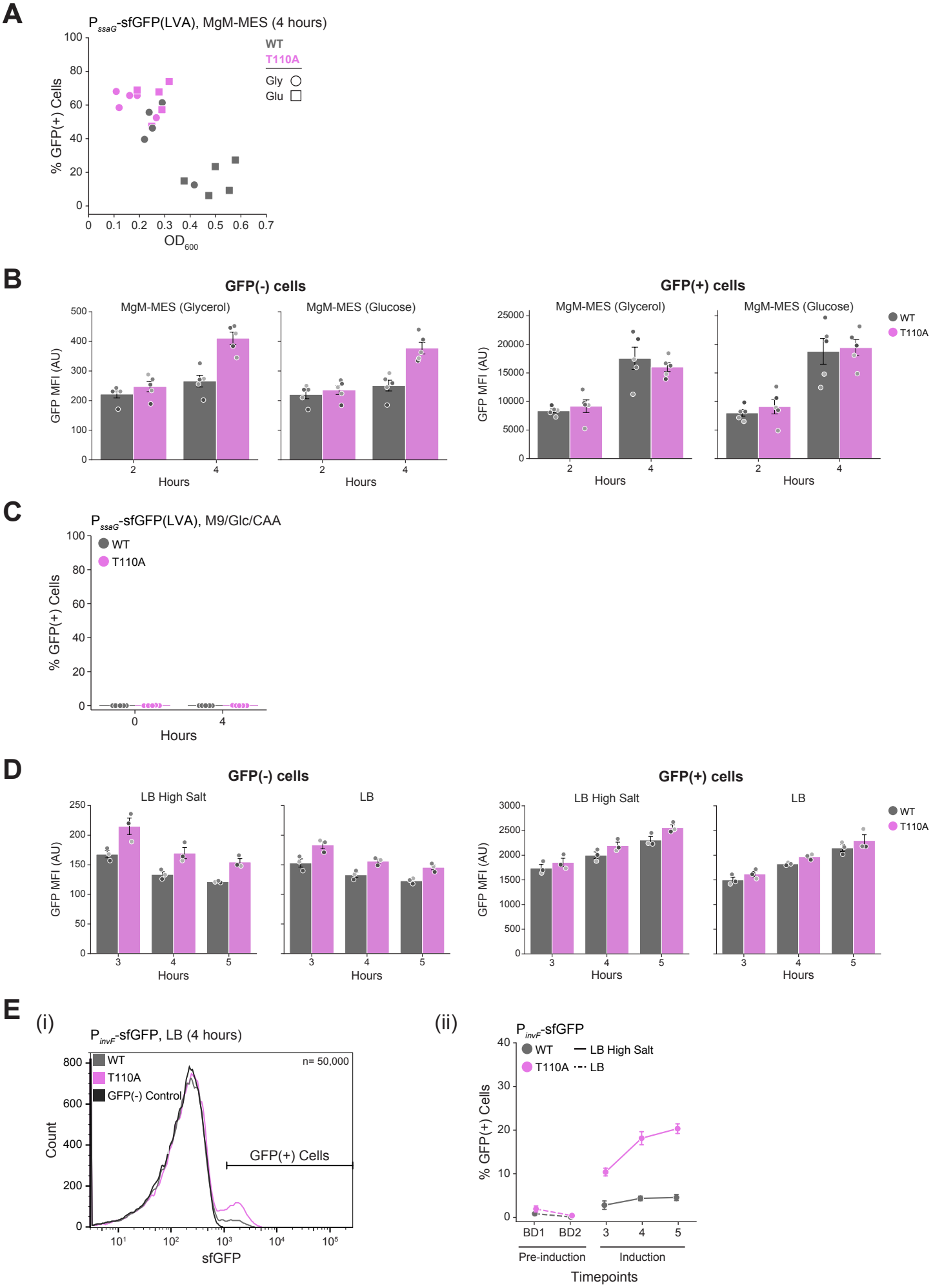
A
P ssaG-sfGFP(LVA), MgM-MES (4 hours)
WT
T110A
Gly
Glu
% GFP(+) Cells
OD600
B
GFP(-) cells
GFP(+) cells
MgM-MES (Glycerol)
MgM-MES (Glucose)
GFP MFI (AU)
Hours
WT
T110A
C
P ssaG-sfGFP(LVA), M9/Glc/CAA
WT
T110A
% GFP(+) Cells
Hours
D
GFP(-) cells
GFP(+) cells
LB High Salt
LB
GFP MFI (AU)
Hours
WT
T110A
E
(i)
P invF-sfGFP, LB (4 hours)
WT
T110A
GFP(-) Control
n= 50,000
GFP(+) Cells
Count
sfGFP
(ii)
P invF-sfGFP
WT
T110A
LB High Salt
LB
% GFP(+) Cells
BD1
BD2
Pre-induction
Induction
Timepoints

Figure 4. *hns* genotype constrains adaptive mutations that improve fitness in SPI-2 inducing conditions. (A) Experimental evolution reveals fitness gains in both WT and T110A strains. (i) Schematic showing the experimental evolution approach. Six individual colonies from each of the WT and T110A strains were inoculated into M9/Glc/CAA overnight, then subcultured daily in 25 mL SPI-2 inducing media (MgM-MES) for 30 days. Glycerol stocks were made daily. Evolved clones at day 5 (d5) and day 30 (d30) were assessed for growth and genotype using plate reader assays and whole genome sequencing. (ii) Growth dynamics of evolved clones. Most T110A clones (shades of blue) show increased fitness by d5 that stabilizes by d30, while WT clones (shades of green) remain similar to the ancestral WT strain at d5 but show increased fitness by d30. Strains were grown in MgM-MES and OD_{600} was recorded using a plate reader. Growth curves show means of three technical replicates, and shaded regions represent standard deviation. Ancestral strains (WT - gray, T110A - magenta) and media control (black) are shown in each plot for comparison. Representative experiments for d5 and d30 are shown. (iii) Growth metrics extracted from data in (ii) and Figure S4A. Circles represent WT (green) and T110A (blue) evolved clones; dashed lines represent means of the ancestral WT and T110A strains; shading indicates variation between two replicates. (B) WT and T110A evolved clones acquire distinct mutations by d30. Genomic DNA from d30 evolved clones was sequenced and mutations are displayed as a clustered heatmap. WT and T110A clones cluster separately (except T110A clone 4). Colorbars indicate ancestral strain (WT - gray, T110A - magenta) and *hns* genotype at d30 (WT - green, T110A - blue). Dark blue in the heatmap indicates the presence of a mutation in the indicated gene, while light gray indicates no mutation. (C) Evolved clones show negligible SPI-2 induction. SPI-2 induction was assessed in two d30 clones from each background (WT clones 3 and 5; T110A clones 2 and 5) using the SPI-2 GFP reporter plasmid (P_{ssaG}-sfGFP(LVA)). Samples were analyzed by flow cytometry after 4 hours in MgM-MES and the percentage of GFP(+) cells compared to that in the ancestral WT and T110A strains. Ancestral strains with GFP(-) control plasmids are shown as a reference for background fluorescence values.

Figure S4. Growth, genotype, and SPI-2 reporter expression of evolved clones. (A) Biological replicate of growth curves for WT and T110A evolved clones at d5 and d30 (related to Figure 4A (ii)). (B) Summary of mutations in WT and T110A clones at d5 and d30. Three T110A clones (clones 1, 3, and 4) were sequenced at d5, while all six clones from each background were sequenced at d30. T110A clone 1 d5 had no mutations, but did have some new junction evidence as detailed in Table S1. (C) Loss of SPI-2 induction in evolved clones (related to Figure 4C). (i) Samples were analyzed by flow cytometry after 4 hours in MgM-MES and the percentage of

GFP(+) cells is shown. Values represent mean ± standard deviation from four independent experiments. (ii) Mean fluorescence intensity (MFI) of GFP(+) cells. Only T110A clone 2 GFP(+) cells have GFP intensity comparable to the original WT and T110A strains. Other evolved clones show intensities similar to the GFP(-) control, indicating loss of SPI-2 induction. Data shown is mean ± standard deviation of 3 independent experiments. n=50,000 cells per sample for each replicate.

Figure 4

A

(i)

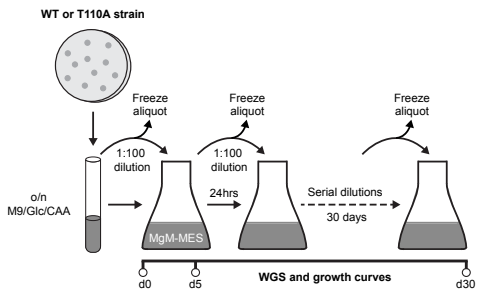

(ii)

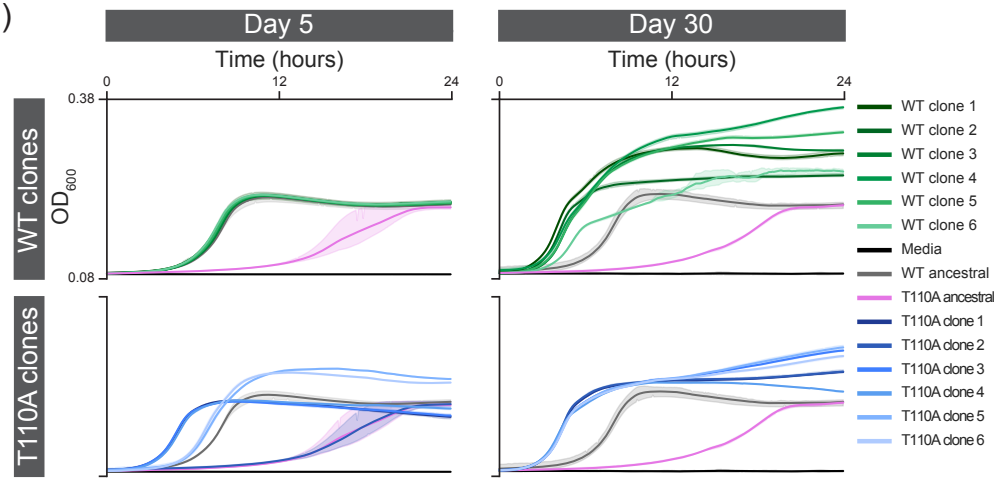

(iii)

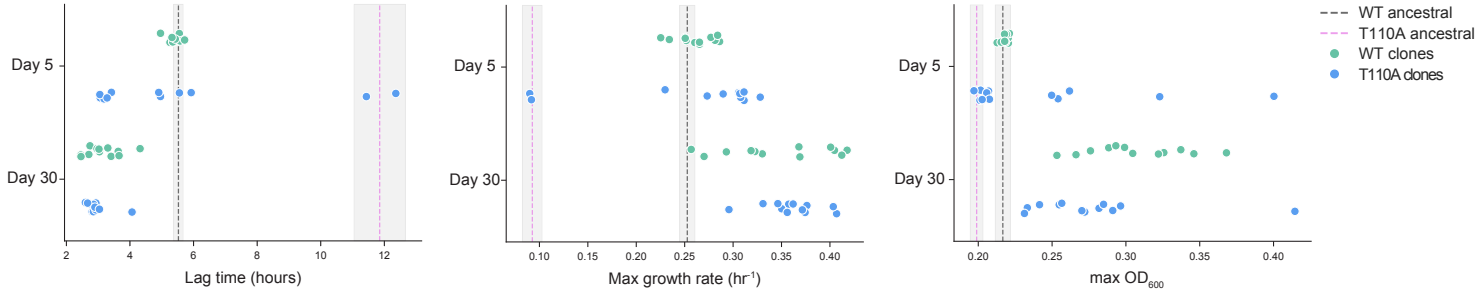

B

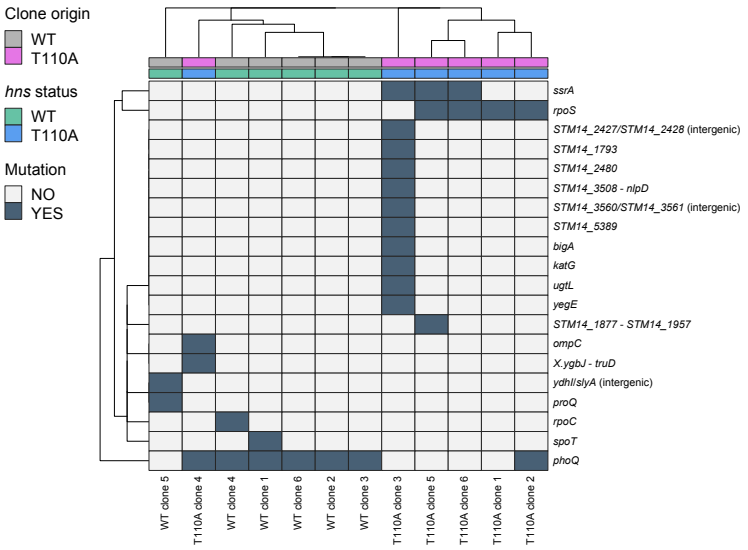

C

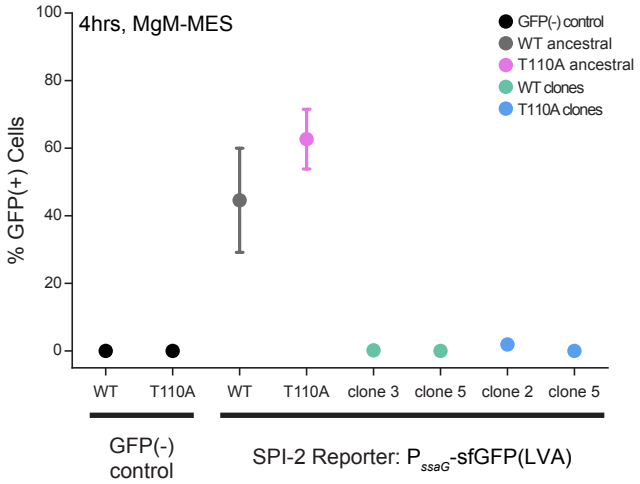

Figure S4

A

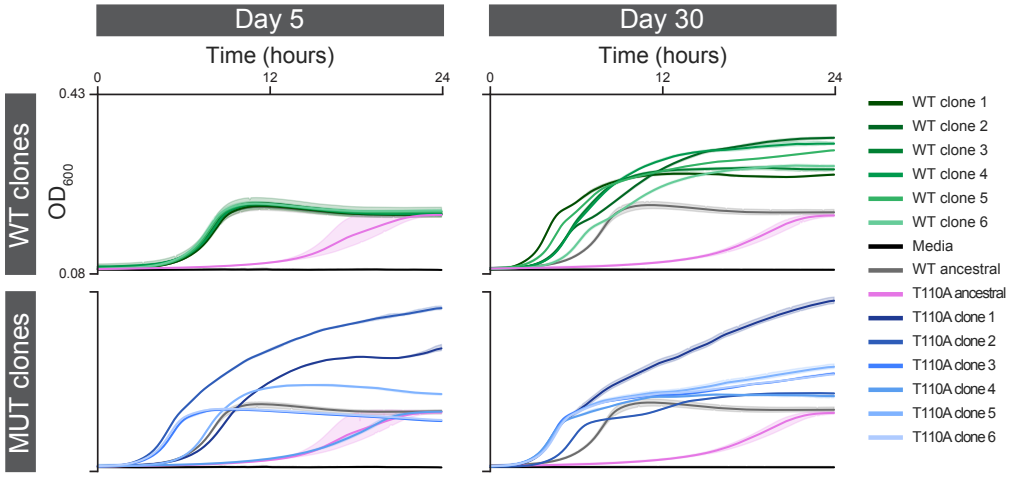
Day 5
Day 30
Time (hours)
Time (hours)
0
12
24
0
12
24
0.43
0.08
OD_{600}
WT clones
MUT clones
WT clone 1
WT clone 2
WT clone 3
WT clone 4
WT clone 5
WT clone 6
Media
WT ancestral
T110A ancestral
T110A clone 1
T110A clone 2
T110A clone 3
T110A clone 4
T110A clone 5
T110A clone 6

Figure S4

B

Summary of genetic changes in WT and T110A lineages

Clone name	Day	Position	Mutation	Annotation	Mutation type	Gene	Description
T110A clone 1	30	3085976	Δ75 bp	coding (674-748/993 nt)	deletion	*rpoS* ←	RNA polymerase sigma factor RpoS
T110A clone 2	30	3086289	Δ68 bp	coding (368-435/993 nt)	deletion	*rpoS* ←	RNA polymerase sigma factor RpoS
T110A clone 2	30	1276242	G→A	P441L (CCA→CTA)	missense	*phoQ* ←	sensor protein PhoQ
T110A clone 3	30	3068653	Δ18,383 bp		deletion	STM14_3508–*nlpD*	STM14_3508, pphB, STM14_3510, mutS, STM14_3512, STM14_3513, STM14_3514, STM14_3515, STM14_3516, ygbM, ygbL, ygbK, ygbJ, ygbI, STM14_3522, STM14_3523, STM14_3524, STM14_3525, rpoS, nlpD
T110A clone 3	30	1488420	(T)7→8	coding (1155/2763 nt)	frameshift ins	*ssrA* ←	sensor kinase SsrA
T110A clone 3	30	1571704	(C)7→8	coding (64/822 nt)	frameshift ins	STM14_1793 ←	putative protease
T110A clone 3	30	1701496	(A)7→8	coding (126/399 nt)	frameshift ins	*ugtL* ←	hypothetical protein
T110A clone 3	30	2094180	(C)7→8	intergenic (-53/-160)	non-coding	STM14_2427 ← / → STM14_2428	hypothetical protein/hypothetical protein
T110A clone 3	30	2130628	T→C	A99A (GCT→GCC)	silent	STM14_2480 →	hypothetical protein
T110A clone 3	30	2260732	C→T	T217M (ACG→ATG)	missense	*yegE* →	putative diguanylate cyclase/phosphodiesterase
T110A clone 3	30	3121521	(A)9→8	intergenic (+63/-305)	non-coding	STM14_3560 → / → STM14_3561	hypothetical protein/putative fimbrial subunit
T110A clone 3	30	3530476	G→A	G388G (GGG→GGA)	silent	*degQ* →	serine endoprotease
T110A clone 3	30	3643324	(C)7→6	coding (296/5895 nt)	frameshift del	*bigA* →	putative surface-exposed virulence protein
T110A clone 3	30	4333233	(G)7→8	coding (66/2181 nt)	frameshift ins	*katG* →	hydroperoxidase
T110A clone 3	30	4753979	(G)7→8	coding (224/2598 nt)	frameshift ins	STM14_5389 ←	putative cytoplasmic protein
T110A clone 3	5	3086014	Δ1 bp	coding (710/993 nt)	frameshift del	*rpoS* ←	RNA polymerase sigma factor RpoS
T110A clone 4	30	3080976	Δ9,307 bp		deletion	*ygbJ*–*truD*	ygbJ, ygbI, STM14_3522, STM14_3523, STM14_3524, STM14_3525, rpoS, nlpD, STM14_3528, pcm, surE, truD
T110A clone 4	30	1276890	G→A	A225V (GCG→GTG)	missense	*phoQ* ←	sensor protein PhoQ
T110A clone 4	30	2417961	G→A	R58C (CGT→TGT)	missense	*ompC* ←	outer membrane porin protein C
T110A clone 4	5	1641701	Δ63,657 bp		deletion	STM14_1877–*ydcP*	STM14_1877, STM14_1878, STM14_1879, STM14_1880, STM14_1881, STM14_1882, STM14_1883, STM14_1884, hdeB, osmC, yddX, rpsV, sfcA, STM14_1890, adhP, fdnI, fdnH, fdnG, STM14_1895, yddG, STM14_1897, nmpC, STM14_1899, smvA, STM14_1901, STM14_1902, narU, STM14_1904, narZ, narY, narW, narV, yddE, nhoA, STM14_1911, STM14_1912, STM14_1913, STM14_1914, STM14_1915, ansP, STM14_1917, STM14_1918, STM14_1919, yncD, yncC, STM14_1922, STM14_1923, yncB, yncA, ydcZ, ydcY, srfA, srfB, srfC, ydcX, STM14_1932, STM14_1933, ydcW, ydcR, pdgL, STM14_1937, ugtL, STM14_1939, sifB, yncJ, ydcP
T110A clone 5	30	1640229	Δ77,091 bp		deletion	STM14_1877–STM14_1957	STM14_1877, STM14_1878, STM14_1879, STM14_1880, STM14_1881, STM14_1882, STM14_1883, STM14_1884, hdeB, osmC, yddX, rpsV, sfcA, STM14_1890, adhP, fdnI, fdnH, fdnG, STM14_1895, yddG, STM14_1897, nmpC, STM14_1899, smvA, STM14_1901, STM14_1902, narU, STM14_1904, narZ, narY, narW, narV, yddE, nhoA, STM14_1911, STM14_1912, STM14_1913, STM14_1914, STM14_1915, ansP, STM14_1917, STM14_1918, STM14_1919, yncD, yncC, STM14_1922, STM14_1923, yncB, yncA, ydcZ, ydcY, srfA, srfB, srfC, ydcX, STM14_1932, STM14_1933, ydcW, ydcR, pdgL, STM14_1937, ugtL, STM14_1939, sifB, yncJ, ydcP, ydcN, STM14_1944, STM14_1945, tehB, tehA, ydcK, rimL, STM14_1950, STM14_1951, STM14_1952, STM14_1953, STM14_1954, STM14_1955, STM14_1956, STM14_1957
T110A clone 5	30	1487862	Δ1 bp	coding (1713/2763 nt)	frameshift del	*ssrA* ←	sensor kinase SsrA
T110A clone 5	30	3086584	G→T	S47* (TCG→TAG)	nonsense	*rpoS* ←	RNA polymerase sigma factor RpoS
T110A clone 6	30	1489105	+A	coding (470/2763 nt)	frameshift ins	*ssrA* ←	sensor kinase SsrA
T110A clone 6	30	3086347	C→T	G126E (GGG→GAG)	missense	*rpoS* ←	RNA polymerase sigma factor RpoS
WT clone 1	30	1277518	G→A	R16C (CGT→TGT)	missense	*phoQ* ←	sensor protein PhoQ
WT clone 1	30	3948939	C→A	P393Q (CCG→CAG)	missense	*spoT* →	bifunctional (p)ppGpp synthetase II/ guanosine-3',5'-bis pyrophosphate 3'-pyrophosphohydrolase
WT clone 2	30	1276242	G→A	P441L (CCA→CTA)	missense	*phoQ* ←	sensor protein PhoQ
WT clone 3	30	1277517	C→A	R16L (CGT→CTT)	missense	phoQ ←	sensor protein PhoQ
WT clone 4	30	1277396	G→C	S56R (AGC→AGG)	missense	phoQ ←	sensor protein PhoQ
WT clone 4	30	4383750	C→A	R53S (CGT→AGT)	missense	rpoC →	DNA-directed RNA polymerase subunit beta'
WT clone 5	30	1529853	G→T	intergenic (-192/-9)	non-coding	ydhI ← / → slyA	putative inner membrane protein/transcriptional regulator SlyA
WT clone 5	30	1955184	C→A	G37V (GGT→GTT)	missense	proQ ←	putative solute/DNA competence effector
WT clone 6	30	1276612	T→A	I318F (ATC→TTC)	missense	phoQ ←	sensor protein PhoQ

C

(i)

% SPI-2 Reporter ON cells

Strain	Reporter	Mean % GFP(+)
WT	GFP(-) control	0.0095 ± 0.0038
T110A	GFP(-) control	0.0060 ± 0.0043
WT	SPI-2 reporter	44.5750 ± 15.409
T110A	SPI-2 reporter	62.6750 ± 8.8300
WT clone 3	SPI-2 reporter	0.1785 ± 0.1414
WT clone 5	SPI-2 reporter	0.012 ± 0.0071
T110A clone 2	SPI-2 reporter	1.91 ± 0.5549
T110A clone 5	SPI-2 reporter	0.007 ± 0.0041

(ii)

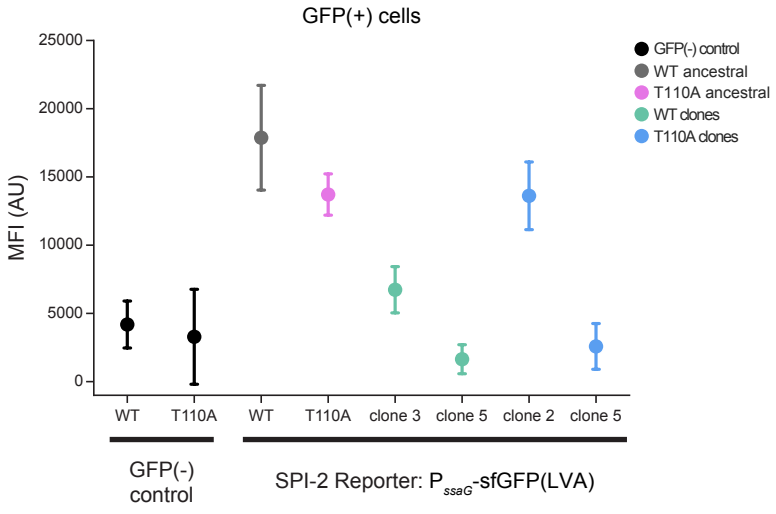

Table S1. Summary of whole genome sequencing results corresponding to data in Figures 1 and 4.

Table S2. Summary of data used for figures and statistical analyses.

Table S3. Reagents.

REAGENT or RESOURCE	SOURCE	Catalog #
***Salmonella* Strains**		
Salmonella enterica serovar Typhimurium 14028 WT	Michael McClelland Lab	
Salmonella enterica serovar Typhimurium 14028 *hns* A328G (T110A)	This Study	
***Salmonella* Cell Culture**		
LB broth, Miller	Fisher Scientific	BP1426
LB broth, Lennox	Fisher Scientific	BP1427
BactoAgar	Fisher Scientific	DF0140-01-0
BD DIFCO™ Nutrient Agar	Fisher Scientific	DF0001-17-0
BD Difco™ Dehydrated Culture Media: M9 Minimal Salts, 5x	Fisher Scientific	DF0485-17
Calcium chloride dihydrate, for molecular biology, ≥99.0%	Sigma-Aldrich	C3306
Magnesium sulfate heptahydrate, BioReagent, for molecular biology, suitable for plant cell culture, ≥99.0%	Sigma-Aldrich	M2773
D-(+)-Glucose,powder, BioReagent, suitable for cell culture, suitable for insect cell culture, suitable for plant cell culture, ≥99.5%	Sigma-Aldrich	G7021
Casamino Acids	Fisher Scientific	BP1424
Potassium chloride, for molecular biology, ≥99.0%	Sigma-Aldrich	P9541
Ammonium sulfate, for molecular biology, ≥99.0%	Sigma-Aldrich	A4418
Potassium sulfate, BioXtra, ≥99.0%	Sigma-Aldrich	P9458
Potassium phosphate monobasic, for molecular biology, ≥98.0%	Sigma-Aldrich	P9791
Mes hydrate,BioPerformance Certified, suitable for cell culture, ≥99.5%	Sigma-Aldrich	M2933
Glycerol	Fisher Scientific	BP229-1
Magnesium chloride hexahydrate, BioReagent, suitable for cell culture, suitable for insect cell culture	Sigma-Aldrich	M2393
Cloning		
PrimeSTAR Max 2X Premix DNA Polymerase	Takara Bio	R045B
EcoFlex MoClo Kit	Addgene	Kit # 1000000080
Mammalian Cell Culture		
HeLa	ATCC	CCL-2

Lenti-X 293T	Takara	632180
DMEM	Fisher Scientific	MT15017CV
Fetal Bovine Serum	Omega Scientific	FB-02
Penicillin/Streptomycin	Fisher Scientific	15-140-122
GlutaMAX	Fisher Scientific	35-050-061
psPAX2	Addgene	Plasmid #12260
pMD2.g	Addgene	Plasmid #12259
Hygromycin	Invivogen	ant-hg-1
Plate Reader		
Glass-bottom 96-well black plate	Tecan	30122306
AeraSeal film	Sigma-Aldrich	A9224
Whole Genome Sequencing		
Wizard(R) Genomic DNA Purification Kit	Promega	A1120
Protein Expression and Purification		
BL21(DE3) Competent Cells	Thermo Fisher Scientific	EC0114
IPTG (Gold Biotechnology Inc)	Fisher Scientific	50-153-2804
Sodium chloride	Sigma-Aldrich	S5886-1KG
DL-Dithiothreitol,for molecular biology, ≥98% (HPLC), ≥99% (titration)	Sigma-Aldrich	D9779-5G
Phenylmethylsulfonyl Fluoride	Fisher Scientific	52-332-5GM
cOmplete™, Mini, EDTA-free Protease Inhibitor Cocktail	Sigma-Aldrich	11836170001
Polyethyleneimine, approx. M.N. 60,000, 50 wt.% aq. solution, branched	Fisher Scientific	AC178571000
1-(3-Aminopropyl)imidazole 97.0+%	Fisher Scientific	A1185100G
2-Mercaptoethanol,for molecular biology, for electrophoresis, suitable for cell culture, BioReagent, 99% (GC/titration)	Sigma-Aldrich	M3148-100ML
Invitrogen Ni-NTA Agarose	Fisher Scientific	R90101
Sodium phosphate dibasic	Sigma-Aldrich	S3264-500G
Corning™ Cell Culture Phosphate Buffered Saline (1X)	Fisher Scientific	MT21040CV
PreScission Protease	Brickner Lab	
Amicon Ultra Centrifugal Filter, 3 kDa MWCO	Sigma-Aldrich	UFC500396
Glycine	Sigma-Aldrich	G8898-500G
Trizma® base	Sigma-Aldrich	93362-250G
Sodium dodecyl sulfate	Sigma-Aldrich	L3771-500G
2x Laemmli Sample Buffer	Bio-Rad	1610737
4–15% Mini-PROTEAN® TGX™ Precast Protein Gels, 15-well, 15 µl	Bio-Rad	4561086
Precision Plus Protein™ Kaleidoscope™ Prestained Protein Standards	Bio-Rad	1610375
Bio-Safe Coomassie Stain	Bio-Rad	1610786
EMSAs		
DNA Clean & Concentrator-5	Zymo Research	D4004

Bromophenol Blue	Fisher Scientific	AAA1846909
Electrophoretic Mobility-Shift Assay (EMSA) Kit, with SYBR™ Green & SYPRO™ Ruby EMSA stains	Fisher Scientific	E33075
5% Mini-PROTEAN® TBE Gel, 15 well, 15 µl	Bio-Rad	4565016
Thermo Scientific™ LightShift™ Poly (dI-dC)	Fisher Scientific	PI20148E
Flow Cytometry		
Electron Microscopy Sciences 16% Paraformaldehyde Aqueous Solution, EM Grade	Fisher Scientific	50-980-487
Microscopy		
Fluorobrite DMEM	Fisher Scientific	A1896701
Fibronectin	Sigma-Aldrich	F0895
Cellvis 96 Well glass bottom plate with high performance #1.5 cover glass	Fisher Scientific	NC0536760
Gibco™ Gentamicin (10 mg/mL)	Fisher Scientific	15-710-064
Software and Algorithms		
Python3	https://www.python.org/	
Seaborn	https://seaborn.pydata.org	
Matplotlib	https://matplotlib.org/	
Cellpose3	https://github.com/MouseLand/cellpose	
CellTK	https://github.com/braysia/CellTK	
Napari	https://napari.org/stable/	
nsbatwm	https://github.com/haesleinhuepf/napari-segment-blobs-and-things-with-membranes	
clEsperanto	https://github.com/clEsperanto	
Breseq	https://github.com/barricklab/breseq/	
FlowJo	v10.8.2	
Omniplate	https://git.ecdf.ed.ac.uk/pswain/omniplate	
ChimeraX	https://www.rbvi.ucsf.edu/chimerax/	
Fiji	https://imagej.net/software/fiji/	

Table S4. Plasmids and Bacterial Strains

Table S4.1

Plasmids			
Plasmid Contents	**Description**	**Antibiotic Resistance**	**Source**
pTU2-a-PssaG-RiboJ-Bba_B0064-sfGFP-LVA-L3S2P21-SJM901-PET_RBS-mRuby2-Bba_B0012-KanR-pSC101	P_{ssaG}-sfGFP-LVA (SPI-2 Reporter)	Kanamycin	Spratt *et al.* (2025)
pTU2-a-PinvF-RiboJ-Bba_B0064-sfGFP-L3S2P21-SJM901-PET_RBS-mRuby2-Bba_B0012-KanR-pSC101	P_{invF}-sfGFP (SPI-1 Reporter)	Kanamycin	This study
pTU2-a-PROMOTERLESS-sfGFP-L3S2P21-SJM901-PET_RBS-mRuby2-Bba_B0012-KanR-pSC101	Promoterless Control Plasmid	Kanamycin	Spratt *et al.* (2025)
pTU1-B-SJM901-PET_RBS-mRuby2-Bba_B0012-AmpR-pSC101	P_{SJM901}-mRuby2 (Constitutive mRuby2)	Carbenicillin	Spratt *et al.* (2025)
pET-28a-H-NS-WT-PPX-6xHis	H-NS WT expression plasmid	Kanamycin	This study
pET-28a-H-NS-T110A-PPX-6xHis	H-NS T110A expression	Kanamycin	This study

Table S4.2

Bacterial Strains		
Strain contents	**Description**	**Source**
STm 14028 WT P_{ssaG}-sfGFP-LVA	WT with SPI-2 reporter plasmid	Spratt *et al.* (2025)
STm 14028 *hns* a328g P_{ssaG}-sfGFP-LVA	T110A with SPI-2 reporter plasmid	This study
STm 14028 WT P_{invF}-sfGFP	WT with SPI-1 reporter plasmid	This study
STm 14028 *hns* a328g P_{invF}-sfGFP	T110A with SPI-1 reporter plasmid	This study
STm 14028 WT Promoterless Control Plasmid	WT with Promoterless control plasmid	Spratt *et al.* (2025)
STm 14028 *hns* a328g Promoterless Control Plasmid	T110A with Promoterless control plasmid	This study
STm 14028 WT P_{SJM901}-mRuby2	WT with Constitutive mRuby2 plasmid	Spratt *et al.* (2025)
STm 14028 *hns* a328g P_{SJM901}-mRuby2	T110A with Constitutive mRuby2	This study
STm 14028 WT evolved clone 1	WT evolved clone 1 Day 30	This study
STm 14028 WT evolved clone 2	WT evolved clone 2 Day 30	This study
STm 14028 WT evolved clone 3	WT evolved clone 3 Day 30	This study
STm 14028 WT evolved clone 4	WT evolved clone 4 Day 30	This study
STm 14028 WT evolved clone 5	WT evolved clone 5 Day 30	This study
STm 14028 WT evolved clone 6	WT evolved clone 6 Day 30	This study
STm 14028 *hns* a328g evolved clone 1	T110A evolved clone 1 Day 30	This study
STm 14028 *hns* a328g evolved clone 2	T110A evolved clone 2 Day 30	This study
STm 14028 *hns* a328g evolved clone 3	T110A evolved clone 3 Day 30	This study
STm 14028 *hns* a328g evolved clone 4	T110A evolved clone 4 Day 30	This study
STm 14028 *hns* a328g evolved clone 5	T110A evolved clone 5 Day 30	This study

STm 14028 *hns* a328g evolved clone 6	T110A evolved clone 6 Day 30	This study
STm 14028 WT evolved clone 3 P_{ssaG}-sfGFP-LVA	WT evolved clone 3 Day 30 with SPI-2 reporter plasmid	This study
STm 14028 WT evolved clone 5 P_{ssaG}-sfGFP-LVA	WT evolved clone 5 Day 30 with SPI-2 reporter plasmid	This study
STm 14028 *hns* a328g evolved clone 2 P_{ssaG}-sfGFP-LVA	T110A evolved clone 2 Day 30 with SPI-2 reporter plasmid	This study
STm 14028 *hns* a328g evolved clone 5 P_{ssaG}-sfGFP-LVA	T110A evolved clone 5 Day 30 with SPI-2 reporter plasmid	This study